Modern Trends in Design of Catalysts for Transformation of Biofuels into Syngas and Hydrogen: From Fundamental Bases to Performance in Real Feeds

Vladislav Sadykov * , **Mikhail Simonov** , **Nikita Eremeev and Natalia Mezentseva**

Department of Heterogeneous Catalysis, Boreskov Institute of Catalysis, 630090 Novosibirsk, Russia; smike@catalysis.ru (M.S.); yeremeev21@catalysis.ru (N.E.); mnv@catalysis.ru (N.M.)
* Correspondence: sadykov@catalysis.ru; Tel.: +7-913-903-8312

Abstract: This review considers problems related to design of efficient structured catalysts for natural gas and biofuels transformation into syngas. Their active components are comprised of fluorite, perovskite and spinel oxides or their nanocomposites (both bulk and supported on high surface area Mg-doped alumina or $MgAl_2O_4$) promoted by platinum group metals, nickel and their alloys. A complex of modern structural, spectroscopic and kinetic methods was applied to elucidate atomic-scale factors controlling their performance and stability to coking, such as dispersion of metals/alloys, strong metal-support interaction and oxygen mobility/reactivity as dependent upon their composition and synthesis procedures. Monolithic catalysts comprised of optimized active components loaded on structured substrates with a high thermal conductivity demonstrated high activity and stability to coking in processes of natural gas and biofuels reforming into syngas. A pilot-scale axial reactor equipped with the internal heat exchanger and such catalysts allowed to efficiently convert into syngas the mixture of natural gas, air and liquid biofuels in the autothermal reforming mode at low (~50–100 °C) inlet temperatures and GHSV up to 40,000 h^{-1}.

Keywords: biofuel reforming; structured catalysts; nanocomposite active components; design; mechanism; performance; coking stability

1. Introduction

Production of syngas by methods alternative to steam reforming of methane now attracts a lot of attention due to both environmental and commercial reasons [1,2]. Conversion of oxygenates obtained from biomass and dry reforming of natural gas appear to be most promising [1–3]. In dry reforming of biogas or natural gas containing $CH_4 + CO_2$ these greenhouse gases are transformed into syngas with H_2/CO ratio ~1, which is a suitable feed for Fischer–Tropsch and oxygenates synthesis. Oxygenates obtained from biomass and glycerol- byproduct of biodiesel production are considered as attractive alternatives to fossil fuels for syngas production [1,4,5].

Efficient catalysts of such processes are usually based upon supported noble (Pt, Rh, Ru) or transition (mainly Ni) metals [1–12]. The main problem of these processes is coking of catalysts leading to their deactivation. Even though noble metals are much more stable to coking, their high price makes their broad-scale application impossible. Hence, great efforts were devoted to design of Ni-based catalysts stable to coking. Next approaches were found to be successful.

1. Instead of traditional supports (SiO_2, alumina, zeolites, etc.) use mixed oxides of rare earth and transition metals with variable oxidation states of cations/oxygen stoichiometry. As the result, such oxides with fluorite [13–29], perovskite [30–67] and spinel [68–76] structures as well as their nanocomposites [35,72,73] have sufficient amount of reactive surface/bulk oxygen species characterized also by a high mobility providing their fast migration to metal particles, where they react with activated

fuel molecules, thus preventing coking [71–73]. These oxides are the most promising supports for catalysts of hydrocarbons or oxygenates reforming to syngas without coking [11–77]. Their oxygen mobility can be tuned by changing their composition as well as synthesis procedures [13,32,35].

2. In the case of bimetallic Ni-containing nanoalloys with Ru, Co, Fe, etc. coking is also much smaller than for pure Ni [8]. This is explained by dilution of the alloy surface layers by added atoms, thus preventing clustering of Ni atoms responsible for graphitic carbon nucleation. Moreover, guest metals suppress migration of carbon atoms into the bulk of alloy particle, thus preventing nucleation of carbon fibers at the metal/support interface [8]. While for traditional as well as fluorite-like supports nanoalloys were mainly loaded via impregnation route, for perovskites and spinels both Ni and other metal cations can be incorporated into the mixed oxide lattice during synthesis. Subsequent reduction generates nanocomposites comprised of segregated metal alloy nanoparticles strongly interacting with oxide matrix, which improves coking resistance and stability to sintering [12,54–61]. However, even for Ce–Zr–O fluorites application of such modern method as solvothermal one-pot synthesis in supercritical alcohols [22–24] allowed to provide incorporation of Ni cations into the mixed oxide lattice with the same Ni nanoparticles exsolution in reducing conditions.

3. Suppression of traditional supports (alumina, etc.) acidity by doping with basic cations such as Mg allows to minimize effect of side reactions (especially for such biofuels as ethanol) leading to coking [12,70,75,78–81].

4. Since for perovskite and fluorite oxides their specific surface area is usually not high, to enhance performance and thermal stability of catalysts on their bases they can be supported on $MgAl_2O_4$ [28,78,81] or Mg-doped alumina [82].

For any practical application catalysts for transformation of biofuels into syngas are to be supported as thin layers on heat-conducting monolithic substrates, which allows to minimize or even avoid heat and mass transfer limitations typical for granulated catalysts beds [77–86].

This review is devoted to analysis of these trends in design of catalysts for transformation of biofuels into syngas based on results of our research in frames of international collaboration in last 10 years compared with those published in literature. The most important new aspect of this review is detailed description of oxygen mobility in catalysts of fuels transformation into syngas comprised of mixed oxides with fluorite, perovskite and spinel structures promoted with Ni and Pt-group metals. It is based on application of unique techniques of oxygen isotope heteroexchange of these catalysts with $^{18}O_2$ or $C^{18}O_2$ in the gas phase in flow installations including experiments in the temperature-programmed mode as well as in the steady-state of catalytic reactions (Steady-State Isotope Transients Kinetic Analysis, SSITKA) [18,35,68,69,71,72,87]. Even though it is well known that a high oxygen mobility and reactivity in these catalysts allows to prevent coking in the reactions of biofuels transformation into syngas by a fast transfer of oxygen species to the metal-support interface, where they interact with activated fuels fragments transforming them into syngas, only in our works such strict characteristics of oxygen mobility as oxygen self-diffusion coefficients were systematically estimated using sophisticated software for isotope exchange kinetics data analysis. Atomic-scale features controlling oxygen mobility in these catalysts were elucidated using modern structural and spectroscopic methods, while their surface oxygen bonding strength was estimated by pulse microcalorimetry, which provided foundations for optimization of their compositions and synthesis procedures [78,82,87].

2. Synthesis of Active Components

The method of synthesis should provide a high dispersion of complex oxides along with spatial uniformity of elements distribution in their particles. A lot of methods including co-precipitation, solvothermal method, sol-gel method, Pechini polymeric precursor method, microemulsions, sonochemical method, microwave-assisted self-combustion and

ultrasonic spray pyrolysis were used for synthesis of oxides [30,33,35,36,87]. Among advanced methods, synthesis in flow regimes (including that in supercritical conditions) characterized by continuous generation of nanoparticles appears to be very promising [20–26,87]. Note that single-phase complex oxides (such as ceria-zirconia mixed oxides, etc.) including cations differing by charge and size and, hence, inherent acidity, could not be prepared by traditional precipitation with alkaline solutions added to a mixed metal salts solution [87].

2.1. Pechini Method

Ester polymeric precursors (Pechini) method [88] is based upon using citric acid and ethylene diamine as chelating agents. With ethylene glycol solution single-phase nanocrystalline doped cerium–zirconium oxides [13,18,89], perovskites [31,32,34,35] and spinel oxides [69] were obtained possessing a high spatial uniformity of cations distribution. In the case of aqueous solutions such spatial uniformity was not obtained [62–65]. For preparation of perovskite-fluorite nanocomposites Pechini method was further modified. It was made by adding fluorite oxide nanopowder into the polymeric precursor solution containing cations of perovskite followed by ultrasonic treatment and evaporation. After polymeric matrix decomposition and calcinations under air this provides nanocomposites with a high specific surface area and developed interphases between perovskite and fluorite domains [31].

2.2. Synthesis in Supercritical Alcohols

Complex $Ce_{1-x}Zr_xO_{2-\delta}$ oxides were synthesized in supercritical ethanol and isopropanol using $Zr(OBu)_4$, $ZrOCl_2$ and $Ce(NO_3)_3 \cdot 6H_2O$ solutions in isopropanol at 400–480 °C and pressure 120–140 atm [22–26]. Single-phase samples with uniform spatial distribution of cations were obtained only with solutions containing acetylacetone (AA) with AA/Zr molar ratio 2. This method allowed also to obtain single-phase samples of $Ce_{1-x}Zr_xO_{2-\delta}$ doped with Ti and Nb cations [21,22] as well as to promote them with Ni cations in so-called one-pot route of synthesis [21–24]. In reducing conditions Ni cations are exsolved from the fluorite lattice providing small Ni clusters strongly interacting with support, which helps to suppress coking and sintering.

2.3. Mesoporous Nanocomposites

Specific surface area of perovskites prepared via Pechini method is in the range of 10–15 m^2/g, which is too small for their good performance as active components of structured catalysts. To deal with this problem perovskites were loaded on Mg-doped γ-Al_2O_3 [90] or mesoporous $MgAl_2O_4$ prepared by self-assembly method induced by evaporation (EISA) with copolymer Pluronic P123 [78].

Even though for (Ru + Ni)-promoted doped $MnCr_2O_4$ spinels specific surface areas were reasonably high (~100 m^2/g), to improve their sintering resistance these active components were loaded on Mg-doped γ-Al_2O_3 as well [90].

3. Characterization of Nanocomposite Materials

3.1. Structural Features

For doped ceria and Ce–Zr–O oxides, a complex of modern techniques was applied for studies of their structure. This includes high resolution transmission electron microscopy with elemental mapping, diffraction studies using X-ray synchrotron radiation and neutron diffraction, wide-angle X-ray scattering (WAXS), infrared and Raman spectroscopies. This allowed to elucidate effects of samples chemical composition and preparation procedures on their phase homogeneity, spatial cations distribution in particles, types and concentrations of defects and features of local coordination environment of Ce and Zr cations [73,77,89–98]. For $Ce_{0.5}Zr_{0.5}O_{2-y}$ composition having the highest oxygen mobility, doping with La, Gd, Pr, Sm cations (thus producing $Ln_x(Ce_{0.5}Zr_{0.5})_{1-x}O_{2-y}$ oxides with x = 0.1 ÷ 0.3) stabilizes the pseudo-cubic structure in humid environment and reduces

domain sizes. For these samples the effect of domain boundaries on the oxygen mobility is significant [18,94,95,98].

Prepared in optimized (with addition of AA complexing agent) supercritical conditions $Ce_{0.5}Zr_{0.5}O_{2-y}$ samples have a cubic structure with the crystallite size of ~5.5 nm. Doping by Ti and Nb cations increases oxygen deficiency due to generation of Ce^{3+} cations [21,22]. According to TEM data, nickel oxide particles supported by impregnation (5 wt.%) have sizes from 20 to 40 nm, while for one-pot route they are smaller (~10 nm).

Perovskites of $LnFe_{0.7-x}Ru_xNi_{0.3}O_{3-\delta}$ (Ln = La, Pr, Sm; x = 0–0.1) composition prepared by Pechini method are single-phase rhombohedral samples. Their reduction produces nanocomposites comprised of Ni–Fe–(Ru) nanoalloys and LnO_x situated in the surface layers of remaining Ln–Fe–O particles [32,34,35].

Freshly prepared $Ru/(La_{0.8}Pr_{0.2}Mn_{0.2}Cr_{0.8}O_3$ + 10 wt.% NiO + 10 wt.% YSZ) nanocomposite mainly consists of the perovskite phase, with Ni and Ru cations being mainly dissolved in its surface layers. YSZ disorders perovskite structure and hampers sintering due to interfaces between its nanoparticles and perovskite domains [32].

Perovskite + fluorite (P+F) nanocomposites prepared by optimized procedures [31,35] are characterized by the developed interphase, a higher specific area as compared to the mechanical mixture of P+F phases. Cations redistribution between perovskite and fluorites nanodomains helps to improve oxygen mobility.

Oxides with a spinel structure based on $MnCr_2O_4$ prepared by Pechini method [69,90] have 2–40% of admixture phase with corundum structure due to segregation of $(Mn,Cr)_2O_3$ oxide during annealing in air. Doping with Fe and Zn cations as well as supporting Ru + Ni decrease the content of this admixture due to spinel structure stabilization.

After supporting up to 10 wt.% of spinel, fluorite or perovskite oxides on $MgAl_2O_4$ or 10 wt.% Mg-doped γ-Al_2O_3 followed by supporting Ru + Ni by impregnation when required, epitaxial layers of these oxides are formed along with incorporation of rare-earth and transition metal cations into the surface layers of these supports [78,90]. In reducing conditions Ni–Ru alloy nanoparticles are formed strongly interacting with layers of rare-earth or transition metal oxides on the surface of these high surface area supports [78,90].

3.2. Surface Properties

The most detailed characteristics of the surface of catalysts were obtained with the help of X-ray Photoelectron Spectroscopy (XPS) and Fourier-transformed Infra-red Spectroscopy of adsorbed CO (FTIRS of adsorbed CO). While the first method gives information about the charge state of ions on the surface (as judged by their binding energies (BE) in XPS spectra) as well as their surface concentrations, the second one allows to estimate the number of coordinatively unsaturated sites (metal atoms, cations) as well as their charges reflected in intensities as well as frequencies of carbonyl absorption bands in FTIRS spectra [13,94–97]. Secondary Ions Mass Spectrometry (SIMS) allows to estimate variation of the content of cations along the depth of the surface layer sputtered by the beam of argon ions [13].

For doped Ce–Zr oxides the surface was found to be enriched by large Pr, Ce and La cations as revealed by XPS and SIMS [94,95]. This implies domain boundaries enrichment by the same cations, which could affect their transport properties.

The surface layer of $MnCr_2O_4$ spinel is enriched by Mn as judged by XPS data, which is explained by segregation of Mn^{2+} cations on the surface of spinel obtained by Pechini method, where decomposition of polymeric precursor under contact with air initially occurs in rather reducing conditions [69]. Apparently even after complete oxidation of all organic residues and transformation of charge state of Mn surface cations mainly to 3+ state with an admixture of 4+ state, they remain on the surface as revealed by its enrichment by Mn. This helps to provide a high mobility and reactivity of the surface oxygen having a lower bonding strength with Mn cations than with Cr cations, thus ensuring a high coking resistance of these catalysts in fuels reforming [68,69,71].

For Pt/Ln–Ce–Zr–O catalysts (Ln = La, Pr, Gd) pretreated in O_2 platinum was found to be present in three oxidation states: 0, 2+ and 4+ (XPS binding energies BE equal to

71, 72 and 75 eV, respectively), the content of Pt cations being the highest in the case of Pr-doped samples [13,95,97]. FTIRS of adsorbed CO also revealed several states of Pt on the surface reflected in bands of linear carbonyls Pt^0-CO (νCO 2046–2084 cm^{-1}), Pt^+-CO (νCO 2125–2140 cm^{-1}) and Pt^{2+}-CO (νCO 2170–2180 cm^{-1}) [13,94–98]. FTIRS spectra did not contain bands which could be assigned to Pt^{4+}-CO carbonyls, since these cations are able to oxidize CO even at liquid nitrogen temperature, being reduced to 2+ and 1+ states. For Pt/La–Ce–Zr–O sample the highest concentration of coordinatively unsaturated Pt^{2+} cations was revealed by these methods, which can be explained by their stabilization with strongly basic La cations. Hence, strong metal-support interaction for these catalysts results in stabilization of Pt^{n+} cations on the surface.

For Ni/Ce–Zr–O samples, mainly FTIRS bands of terminal carbonyls Ni-CO at νCO~2105 cm^{-1} are observed [89]. This is explained by decoration of Ni nanoparticles surface by Ce–Zr–O fragments due to strong metal-support interaction, thus hampering appearance of neighboring Ni atoms able to stabilize bridging carbonyls. In a similar way, FTIRS bands corresponding to terminal Ni/Ru carbonyls were mainly observed for Ni + Ru loaded oxides, where alloys are formed after reduction [78,90,91]. Hence, these effects of dilution and decoration are vital to prevent coking, since carbon nucleation on Ni particles requires ensembles of the same surface atoms >6 or stepped faces having coordinatively unsaturated atoms [8].

3.3. Oxygen Species: Bonding Strength and Mobility

The bonding strength of surface oxygen species is determined by such methods as pulsed microcalorimetry and temperature-programmed desorption (TPD) of O_2. Experimental data are compared with calculations for model structures of surface sites using the semiempirical interacting bonds method [35,99–104]. The oxygen mobility was estimated using such methods as oxygen isotope heteroexchange with $^{18}O_2$ or $C^{18}O_2$ [24,68,69,105–107], steady state isotopic transient kinetic analysis (SSITKA) [108,109] and modeling of reforming processes kinetic relaxations [19,104,108].

For catalysts based on fluorite, perovskite and spinel oxides containing transition and rare-earth cations with variable charges, the bonding strength of surface oxygen species depends on their stoichiometry. In the initial oxidized state, it is ~150–200 kJ/mol O_2, corresponding to M–O forms of oxygen [35,99,100]. After removing more than one monolayer of oxygen its binding strength increases to ~400 kJ/mol for spinels ($MnCrO_x$), ~500 kJ/mol for perovskites (PrFeOx, LaPrMnCrOx) and ~650 kJ/mol for LnCeZrO fluorites, respectively, corresponding to M_2O bridging forms of the surface oxygen [99–103]. In the stationary state of these catalysts in the reactions of fuels reforming, only bridging forms of oxygen are present on the surface being regenerated by CO_2 or H_2O pulses forming also CO and H_2 as products [101–103]. For PrCeZrO fluorite and $MnCrO_x$ spinel layers supported on mesoporous $MgAl_2O_4$ the coverage by reactive oxygen species decreases while their bonding strength increases due to interaction with support [104].
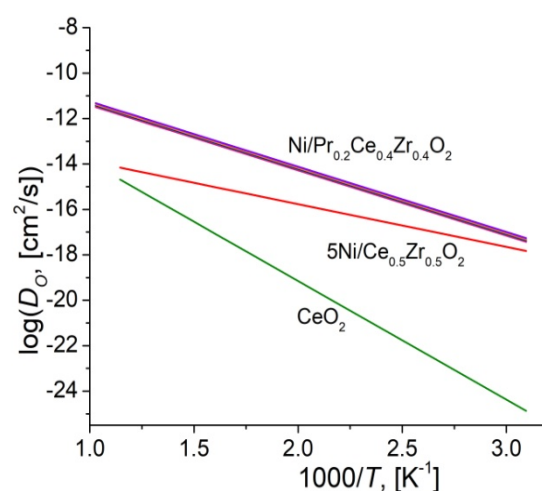
Diffusion coefficients of oxygen for these catalysts are high enough (up to 10^{-12} cm^2/s at 700 °C, Table 1, Figure 1) to provide fast oxygen migration to the metal–support interface, which is required to transform activated fuel fragments into syngas.

Even though for stoichiometric spinel $MnCr_2O_4$ the oxygen diffusion in the bulk is not too fast, it is at least close to that of La-doped ceria-zirconia, which allows to suggest usage of much less expensive spinel for the catalysts design. Oxygen diffusion coefficients along domain boundaries in Pt-supported fluorites exceed by 1–3 order of magnitude those for the bulk diffusion (Table 1). The amount of oxygen involved into this fast diffusion channel decreases when using oxygen exchange with $C^{18}O_2$ or SSITKA instead of heteroexchange with $^{18}O_2$, apparently reflecting also its lower amount (oxygen storage capacity) in real reaction conditions of biofuels reforming.

Table 1. Oxygen self-diffusion coefficients in the bulk (D_{bulk}) and along grain boundaries ($D_{interface}$) at 700 °C [19,24,68,69,104–109].

Sample, Type of Exchange Molecule	D_{bulk}, cm^2/s	$D_{interfaces}$, cm^2/s
Pt/Pr$_{0.3}$Ce$_{0.35}$Zr$_{0.35}$O$_{2-\delta}$, ^{18}O$_2$	4×10^{-14}	$>3.3 \times 10^{-11}$
Pt/Pr$_{0.3}$Ce$_{0.35}$Zr$_{0.35}$O$_{2-\delta}$, C^{18}O$_2$	-	$>2 \times 10^{-12}$
Pt/La$_{0.3}$Ce$_{0.35}$Zr$_{0.35}$O$_{2-\delta}$, ^{18}O$_2$	4×10^{-15}	$5 \times 10^{-13} \div 7 \times 10^{-13}$
LaNiPt/Pr$_{0.15}$Sm$_{0.15}$Ce$_{0.35}$Zr$_{0.35}$O$_{2-\delta}$, ^{18}O$_2$	3×10^{-14}	$>2.5 \times 10^{-11}$
LaNiPt/Pr$_{0.15}$Sm$_{0.15}$Ce$_{0.35}$Zr$_{0.35}$O$_{2-\delta}$, C^{18}O$_2$	-	$>5 \times 10^{-12}$
Co$_{1.8}$Mn$_{1.2}$O$_4$, ^{18}O$_2$	8×10^{-13}	-
Ni$_{0.33}$Co$_{1.33}$Mn$_{1.33}$O$_4$, ^{18}O$_2$	1.5×10^{-12}	-
Ni$_{0.6}$Co$_{1.2}$Mn$_{1.2}$O$_4$, ^{18}O$_2$	10^{-11}	-
PrNi$_{0.5}$Co$_{0.5}$O$_3$–Ce$_{0.9}$Y$_{0.1}$O$_{2-\delta}$-nanocomposite, C^{18}O$_2$	$10^{-11} \div 10^{-9}$	$10^{-8} \div 10^{-7}$
Ce$_{0.65}$Pr$_{0.25}$Y$_{0.1}$O$_{2-\delta}$, C^{18}O$_2$	10^{-8}	-
Ni/Pr$_{0.2}$Ce$_{0.4}$Zr$_{0.4}$O$_{2-\delta}$, C^{18}O$_2$	4.8×10^{-12}	-
Ni$_{0.5}$Cu$_{0.5}$O/Nd$_{5.5}$WO$_{11.25-\delta}$ nanocomposite, C^{18}O$_2$	Fast 2.2×10^{-11} Slow $\sim 10^{-13}$	-
5 wt.% Ni/Ce$_{0.75}$Zr$_{0.25}$O$_2$, C^{18}O$_2$	1.3×10^{-14}	-
2 wt.% Ni+2 wt.% Ru/MnCr$_2$O$_4$, C^{18}O$_2$	2.6×10^{-15}	-

Figure 1. Temperature dependencies of oxygen self-diffusion coefficients D_O for ceria and ceria-zirconia based samples prepared via modified Pechini route.

For PrNi$_{0.5}$Co$_{0.5}$O$_3$–Ce$_{0.9}$Y$_{0.1}$O$_{2-\delta}$ nanocomposite the method of isotopic heteroexchange of oxygen with C^{18}O$_2$ also demonstrated coexistence of fast and slow channels of oxygen diffusion [106]. Fast migrations go through perovskite–fluorite interfaces as well as via Ce$_{0.65}$Pr$_{0.25}$Y$_{0.1}$O$_{2-\delta}$ nanodomains (Table 1), while diffusion through perovskite domains is slow.

4. Catalytic Properties

4.1. Catalysts Based on Cerium–Zirconium Mixed Oxides

In methane dry reforming (MDR) Ni-supported biphasic ceria-zirconia sample prepared in supercritical ethanol without adding AA complexion was very fast completely deactivated in MDR due to coking [20]. In contrary, a high and stable performance of catalysts with Ni supported by impregnation on single-phase Ce$_{0.5}$Zr$_{0.5}$O$_2$ oxide prepared either by modified Pechini route or in supercritical alcohols with addition of AA (*vide supra*)

was maintained even at 600 °C [20–24,89]. At 700 °C, the effective first-order rate constants for these catalysts were in the range of 1–4 s^{-1} cm^{-2}, being close to values for Pt or Ru- supported Pr (Pr+Sm)–doped ceria-zirconia (Figure 2) and exceeding by an order of magnitude k values for Ni supported on these fluorites (~0.2 s^{-1} cm^{-2} at 700 °C) [87]. This stresses importance of the spatial homogeneity of ceria-zirconia mixed oxide for ensuring a high oxygen mobility and, hence, stability to coking, which is usually not taken into account.
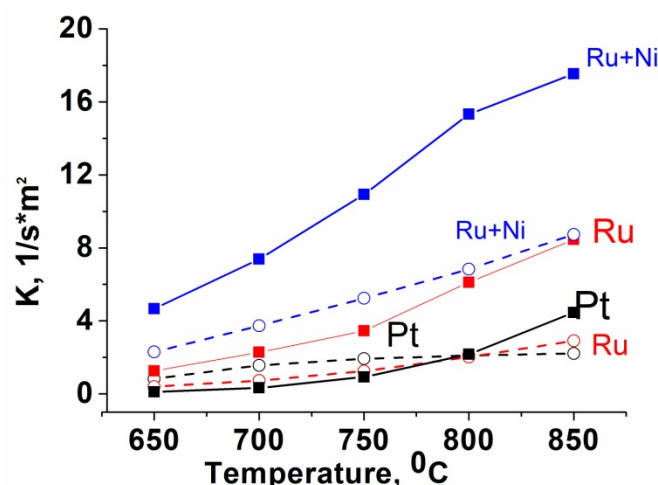
Figure 2. Specific rate constants temperature dependence for methane dry reforming on metal-supported SmPrCeZrO (filled symbols) and PrCeZrO (empty symbols) catalysts. Feed 7% CH$_4$ +7% CO$_2$ in He.

Mixed Ce$_{0.75}$Zr$_{0.25}$O$_2$ oxides doped with Ti, Nb and Ti+Nb (Table 2) were prepared in supercritical isopropanol with addition of AA. 5 wt.% Ni were supported either by impregnation (I) or via one-pot synthesis from mixed solutions in supercritical conditions (O) [24]. For samples with Ni added in one-pot route its surface content estimated as Ni/Ce+Zr atomic ratio from X-ray photoelectron spectroscopy data was twice as low in comparison with impregnated samples. This indicates Ni incorporation into the bulk of fluorite particles for one-pot samples reflected in the increase of oxygen diffusion coefficients (Table 2) due to generation of additional oxygen vacancies. Such disordering also leads to stronger sintering of samples during calcinations step, so specific surface area for one-pot samples was twice as low [24]. However, both reagents' conversions and reaction rate related to the surface concentration of nickel atoms estimated by hydrogen chemisorption (TOF, turn-over frequency) of one-pot samples were quite close to those of impregnated samples of the same chemical composition (Table 2), which indicates on a higher dispersion of Ni on the surface of one-pot samples. TOF values strongly depend on the support composition, and the catalyst with titanium and niobium co-doped ceria-zirconia support prepared by impregnation is three times more active than that with the unmodified ceria-zirconia support, apparently due to optimized interaction of Ni with more disordered doped ceria-zirconia.

Table 2. Kinetic parameters of MDR and oxygen mobility for catalysts prepared in supercritical conditions [24].

Sample [1]	k_{eff} (700 °C), s^{-1}	TOF, s^{-1}	D_O (700 °C), 10^{-15} cm^2/s
5 wt.% Ni/Ce$_{0.75}$Zr$_{0.25}$O$_2$-I	46	2.9	7.1
5 wt.% Ni/Ce$_{0.75}$Zr$_{0.25}$O$_2$-O	51	2.4	13
5 wt.% Ni/Ce$_{0.75}$Ti$_{0.1}$Zr$_{0.15}$O$_2$-I	38	3.4	3.2
5 wt.% Ni/Ce$_{0.75}$Ti$_{0.05}$Nb$_{0.05}$Zr$_{0.15}$O$_2$-I	64	9.0	1.7
5 wt.% Ni/Ce$_{0.75}$Ti$_{0.05}$Nb$_{0.05}$Zr$_{0.15}$O$_2$-O	38	2.6	7.8

[1] I—impregnated sample, O—one-pot sample.

Oxygen diffusion coefficients (D_o) estimated by the isotope exchange method, of the order of 10^{-15}–10^{-14} cm^2/s (Table 2), are quite close to those for Ni/Ce$_{0.5}$Zr$_{0.5}$O$_2$ with single-phase oxide support prepared via modified Pechini route (Figure 1). They are high enough for efficient oxygen transport to the metal-support interface and contribute to a high value of catalytic activity and stability against catalyst coking.

For catalysts based on SmPrCeZrO$_2$ oxide support, in MDR the rate constant was higher for supported Ru (~7 s^{-1} m^{-2} at 850 °C) than for Pt (Figure 2) [87]. Ni-supported catalyst is much less active (k~0.2 s^{-1} cm^{-2} at 700 °C), which is explained by coking of the catalyst. For supported LaNiO$_3$ activity is higher by an order of magnitude (k~1.8 s^{-1} cm^{-2} at 700 °C). This is explained by decoration of Ni nanoparticles by LaO$_x$CO$_3$ species preventing coking. Ru+Ni-supported catalyst demonstrates the highest activity (Figure 2) since NiRu clusters are not coked [87]. For Ru co-supported with LaNiO$_3$, specific activity is significantly lower being identical with that for Ru alone supported on this fluorite. According to CO chemisorption data the metal surface area for this catalyst (~0.05 m^2/g) is much lower than that for Ru + Ni–loaded sample (0.5 m^2/g). Hence, the rate constant related to the metal surface is even higher for Ru+LaNiO$_3$–loaded catalyst due to stronger metal–support interaction/interface.

For Pt/Ln$_x$(Ce$_{0.5}$Zr$_{0.5}$)$_{1-x}$O$_{2-y}$ catalysts specific rate of hydrogen production in methane partial oxidation into syngas (POM) in diluted feed (Figure 3) is the highest for La-doped catalysts due to a higher content of Pt^{n+} cations transformed into clustered metal species in reaction media [13,18,72,94,95].
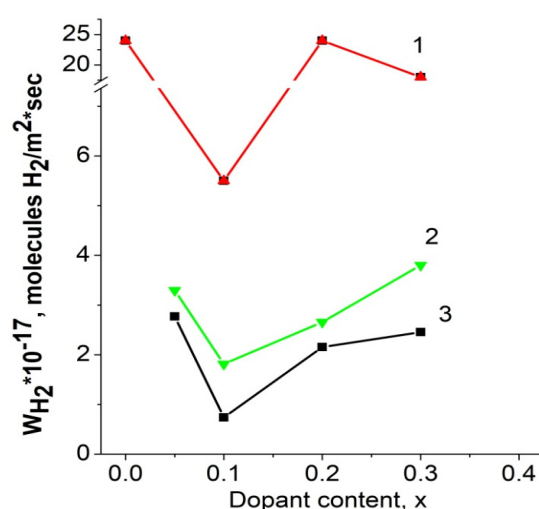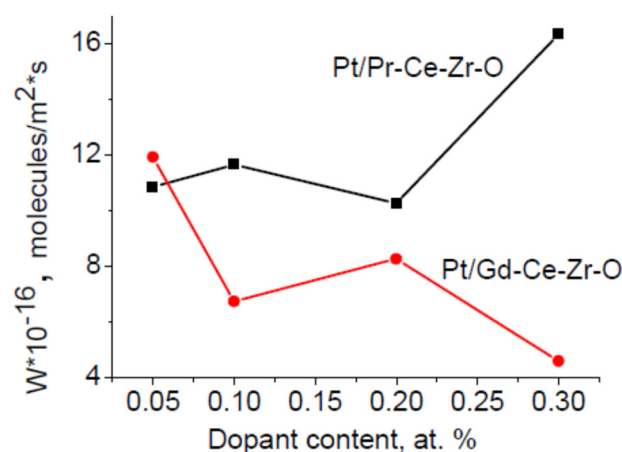

Figure 3. Specific rate of H$_2$ production in partial oxidation of methane for Pt/La$_x$(Ce$_{0.5}$Zr$_{0.5}$)$_{1-x}$O$_{2-y}$ O$_{2-y}$ (1), Pt/Pr$_x$(Ce$_{0.5}$Zr$_{0.5}$)$_{1-x}$O$_{2-y}$ (2) and Pt/Gd$_x$(Ce$_{0.5}$Zr$_{0.5}$)$_{1-x}$O$_{2-y}$ (3) catalysts. Feed 1% CH$_4$ + 0.5% O$_2$ in He, 770 °C, contact time 5 ms.

In the autothermal reforming of acetone (Figure 4) [95], specific catalytic activity of Pt-supported doped ceria-zirconia catalysts correlates with the oxygen mobility required to prevent coking, being the highest for Pt/Pr$_{0.3}$Ce$_{0.35}$Zr$_{0.35}$O$_2$ catalyst [18].

While testing catalysts in real concentrated feeds in POM, methane steam reforming and MDR, the temperature gradient along the length of reactor equipped with the catalyst fraction or granules caused by exothermicity or endothermicity of these reactions emerges, which complicates data analysis. To avoid this problem, catalytic layers were supported onto the inner walls of single channels cut from corundum honeycomb monoliths, which allowed to avoid any temperature gradients and estimate rate constants (Table 3) [109–112]. Among Pt/Ln$_x$(Ce$_{0.5}$Zr$_{0.5}$)$_{1-x}$O$_{2-y}$ catalysts the highest activity was revealed for Pr-doped catalyst possessing the highest oxygen mobility, which stresses importance of this characteristic.

Figure 4. Specific rate of H_2 production in autothermal reforming of acetone for $Pt/Pr_x(Ce_{0.5}Zr_{0.5})_{1-x}O_{2-y}$ and $Pt/Gd_x(Ce_{0.5}Zr_{0.5})_{1-x}O_{2-y}$ catalysts.

Table 3. Effective first-order rate constants (s^{-1}) of CH_4 reforming at 700 °C on separate corundum channels with supported active components [111,112].

Catalyst Composition	Partial Oxidation [1]	Steam Reforming [2]	Dry Reforming [3]
$LaNiO_x/Ce_{0.2}Zr_{0.8}O_2$	80		
$LaNiPt/Ce_{0.2}Zr_{0.8}O_2$ (0.4 wt.% Pt)	63	16	62
0.4 wt.% $Pt/Ce_{0.2}Zr_{0.8}O_2$	40	20	5
0.4 wt.% Pt+2.8 $La/Ce_{0.2}Zr_{0.8}O_2$	94	44	44
1.8 wt.% $Pt/Ce_{0.2}Zr_{0.8}O_2$	40	4	1
1.4 wt.% $Pt/Pr_{0.05}(Ce_{0.5}Zr_{0.5})_{0.95}O$		40	
1.4 wt.% $Pt/Pr_{0.3}Ce_{0.35}Zr_{0.35}O_2$	80	30	30
1.4 wt.% $Pt/Gd_{0.3}Ce_{0.35}Zr_{0.35}O_2$	60		8
1.4 wt.% $Pt/La_{0.3}Ce_{0.35}Zr_{0.35}O_2$	30		4

[1] Feed 7% CH_4 + 3.5% O_2, N_2 balance; [2] Feed 7% CH_4 + 21% H_2O, N_2 balance; [3] Feed 7% CH_4 + 7% CO_2, N_2 balance.

To accelerate preparation of ceria-zirconia based catalysts, an automated workstation was used allowing wet impregnation of La-doped γ-Al_2O_3 by mixed solutions, so series of samples with supported CeZrO layers doped by Pr or Sm and promoted by Pt, Ru, Cu, Cu + Ni were made [113]. The ruthenium-promoted $Ru/Ce_{0.4}Zr_{0.4}Sm_{0.2}O_{2-y}/La$-$\gamma$-$Al_2O_3$ catalyst demonstrated the best activity and coking stability in ethanol steam reforming, which was explained by a high mobility and reactivity of oxygen in this sample.

4.2. Catalysts Based on Perovskite Oxides

4.2.1. Reactions of Methane Reforming

A lot of ABO_3 perovskites with partial substitution of La in A sublattice for alkaline-earth (Ca, Sr) or rare-earth (Ce, Pr) cations as well as containing in B sublattice, along with Ni, such metals as Fe, Co, Rh and Ru, were studied in these reactions [30–48,50,51,53–60] as well as in diesel fuel reforming [49,61]. Main attention was paid to the effect of perovskite initial composition on segregated in reaction conditions Ni (or Ni alloys) dispersion, interaction of a metal component with remaining oxide matrix and ability of the latter to activate oxidants and provide oxygen species diffusion to the metal-support interface. Clearly, formation of Ni nanoalloys with Co, Fe, Ru, Rh for reduced perovskites doped in B sublattice prevents coking. For Fe-containing perovskites [28,32,34,39,57] incomplete reduction of Fe cations in reaction conditions helps to stabilize a part of perovskite Ln-Fe-O matrix strongly interacting with segregated nanoalloys. In a similar way, substitution

of La in A sublattice for Ce and Pr cations able to change their charge state increases oxygen mobility and reactivity in remaining perovskite matrix, thus improving resistance to coking [32,34,58].

A high and stable performance in MDR without any coking was demonstrated also for $LaMnO_3$-based perovskite with *in-situ* exsolved Ni nanoparticles strongly interacting with perovskite surface layers [114].

Detailed review on methane dry reforming over perovskite derived catalysts is presented in [39], where basically the same trends in ensuring high and stable performance related to oxygen mobility and strong interaction of metal nanoparticles with remaining oxide matrix are analyzed.

### 4.2.2. Ethanol Reforming on Bulk Perovskites

In reactions of oxygenates reforming a high activity and stability of catalysts based on perovskites precursors was shown as well [32,63–67,108–110,115,116]. The same factors—exsolution of Ni-containing nanoalloys from perovskite lattice in reducing conditions, their stabilization by strong interaction with remaining matrix and oxygen transfer to metal-support interface determine their resistance to coking and activity. It has been shown that even Ni/La_2O_3 catalysts obtained from $LaNiO_3$ have a higher stability to coking than catalysts of the same composition prepared by traditional impregnation.

In our work [32], $LnFe_{0.7-x}M_xNi_{0.3}O_3$ perovskites (Ln = La, Pr, M = Mn, Ru, x = 0–0.3) as precursors of robust catalysts were prepared by modified Pechini route. Before testing in EtOH steam reforming in concentrated feed 10% EtOH+40% H_2O + N_2 at contact time 70 ms they were either reduced by H_2 at 850 °C or pretreated in the reaction feed. The highest activity was shown by Pr and Ru-containing samples, with specific rate constants at 800 °C varying from 4 to 8 $s^{-1}m^{-2}$, and their performance was stable due to presence of only a trace admixture of ethylene in products, which is usually responsible for coking in this reaction.

4.2.3. Perovskite-Fluorite Nanocomposites

Since perovskite + fluorite nanocomposites possess a higher oxygen mobility compared to separate phases [106], a lot of research was devoted to their design not only as cathodes of solid oxide fuel cells (SOFC) and materials for oxygen separation membranes [35,87], but also as active components of structured catalysts for fuels reforming and SOFC anodes operating in the internal reforming mode [31,32,35,72,73,77,87,117–120]. As fluorites doped ceria or zirconia were employed. Different methods of synthesis were used for preparation, the most efficient was modified Pechini method when prepared nanocrystalline fluorite was dispersed in a polymeric precursor of perovskite followed by its decomposition and calcinations [31], while (100 − x) wt.% $LnFeNi_{0.3}$ + x wt.% $Ce_{0.9}Gd_{0.1}O_{2-\delta}$ (GDC) (x = 5–50 wt.%) nanocomposites were prepared from polymeric precursors containing all cations. Their testing in MDR (feed 10% CH_4 +10% CO_2 in He, contact time 15 ms) revealed that at 800 °C specific first-order rate constant k ($s^{-1}m^{-2}$) goes through the maximum at x = 10 wt.% (k = 5.5), its values being nearly the same at x = 0 (k = 2.5) and 20% (k = 2.0). Such trend is apparently explained by the positive effect of perovskite structure disordering at a low content of fluorite dopant followed by subsequent surface blocking by Ce and Gd cations due to their segregation as a result of their bigger sizes.

Nanocomposite (10 wt.% Ni + 2 wt.% Ru)/($La_{0.8}Pr_{0.2}Mn_{0.2}Cr_{0.8}O_3$ + 10 wt.% YSZ) [72,73,77] showed a high and stable performance in MDR. Its specific activity is close to that of (Ru + Ni)/SmPrCeZrO catalyst (Figure 5a), and it provides a high methane conversion into syngas at high temperatures even at short contact times (Figure 5b).
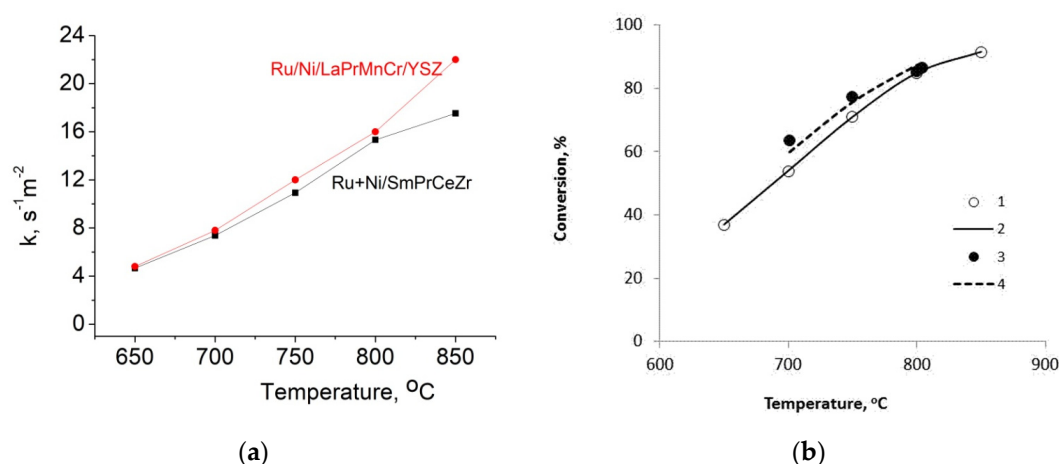
Figure 5. (**a**) Temperature dependence of specific rate constants for methane dry reforming on fractions of (Ru+Ni)/SmPrCeZrO and (Ru+Ni)/LaPrMnCr/YSZ catalysts. Feed 7% CH_4 + 7% CO_2, contact time 15 ms; (**b**) Temperature dependence of CH_4 conversion in CH_4 dry reforming on fraction of (Ru+Ni)/(LaPrMnCr+YSZ) catalyst (1, 2; feed 7% CH_4 + 7% CO_2 in He, contact time 15 ms) and on the stack of microchannel plates with this active component (3, 4; feed 20% CH_4 + 20% CO_2 in Ar, contact time 0.4 s). 1,3-experimental data, 2,4-fitting.

4.3. Catalysts Based on Spinels

$Co_{1.8}Mn_{1.2}O_4$, $Ni_{0.33}Co_{1.33}Mn_{1.33}O_4$ and $Ni_{0.6}Co_{1.2}Mn_{1.2}O_4$ catalysts were prepared by thermal decomposition of nitrates and studied in ethanol steam reforming reaction. The highest activity was found for $Ni_{0.6}Co_{1.2}Mn_{1.2}O_4$ catalyst, which is explained by a high content of mixed Ni-Co clusters segregated at the surface in reaction conditions along with the highest oxygen mobility (Table 1) preventing coking [68].

Mixed manganese-chromium oxides $Mn_xCr_{3-x}O_4$ (x = 0.3–2.7) prepared by modified Pechini route and promoted by 2 wt.% Ni + 2 wt.% Ru were studied in steam reforming of ethanol [69]. The density of surface metal sites was estimated by CO pulse chemisorption. The highest conversion of ethanol and yield of syngas were obtained for stoichiometric $MnCr_2O_4$ composition. Turnover frequencies (TOF, s^{-1}) at 500 °C vary in the row (Ru+Ni)/$Mn_{0.3}Cr_{2.7}O_4$ (0.88) < (Ru+Ni)/Mn_2CrO_4 (1.13) < (Ru+Ni)/$Mn_{2.7}Cr_{0.3}O_4$ (1.36) < (Ru+Ni)/$MnCr_2O_4$ (3.28). In this series of catalysts, the highest oxygen diffusion coefficient was found for (Ru+Ni)/$Mn_{2.7}Cr_{0.3}O_4$ sample with the excess of manganese. This implies that namely metal-support interaction provides the highest TOF for (Ru+Ni) $MnCr_2O_4$ catalyst, while sufficient oxygen mobility (Table 1) ensures coking stability. Even in concentrated feed 10% C_2H_5OH + 40% H_2O in N_2 at short contact time 70 ms concentration of byproduct CH_4 was only 2% at 700 °C, while only trace admixtures of usual byproducts such as ethylene and acetaldehyde were observed [69]. This means that such known intermediates as ethoxy complexes and acetaldehyde are rapidly transformed into syngas due to a high concentration of reactive oxygen forms and metal sites [104,121].

Testing (Ru + Ni)/$MnCr_2O_4$ catalyst in the autothermal reforming of glycerol (feed 10.9% $C_3H_8O_3$ + 9.5% O_2 + 44.5% H_2O + 35.1% N_2, contact time ~40 ms) also revealed its high efficiency and stable performance [73]. Thus, already at 750 °C complete conversion of glycerol was achieved with the content of main byproducts CH_4 and C_2H_4 less than 2% and syngas yield approaching equilibrium.

4.4. Catalysts Based on High Surface Area Supports

Since specific surface area of perovskites, fluorites and spinel is lower than that of traditional supports such as γ-alumina, silica, zeolites, etc., a lot of research was devoted to design of catalysts for fuels reforming where active components—metals or their combination with reactive oxides are loaded on high surface area supports [12,28,39,72,75,77–80,90,122–133]. Since acidity of supports is well known to be responsible for coking, the best results for activity and
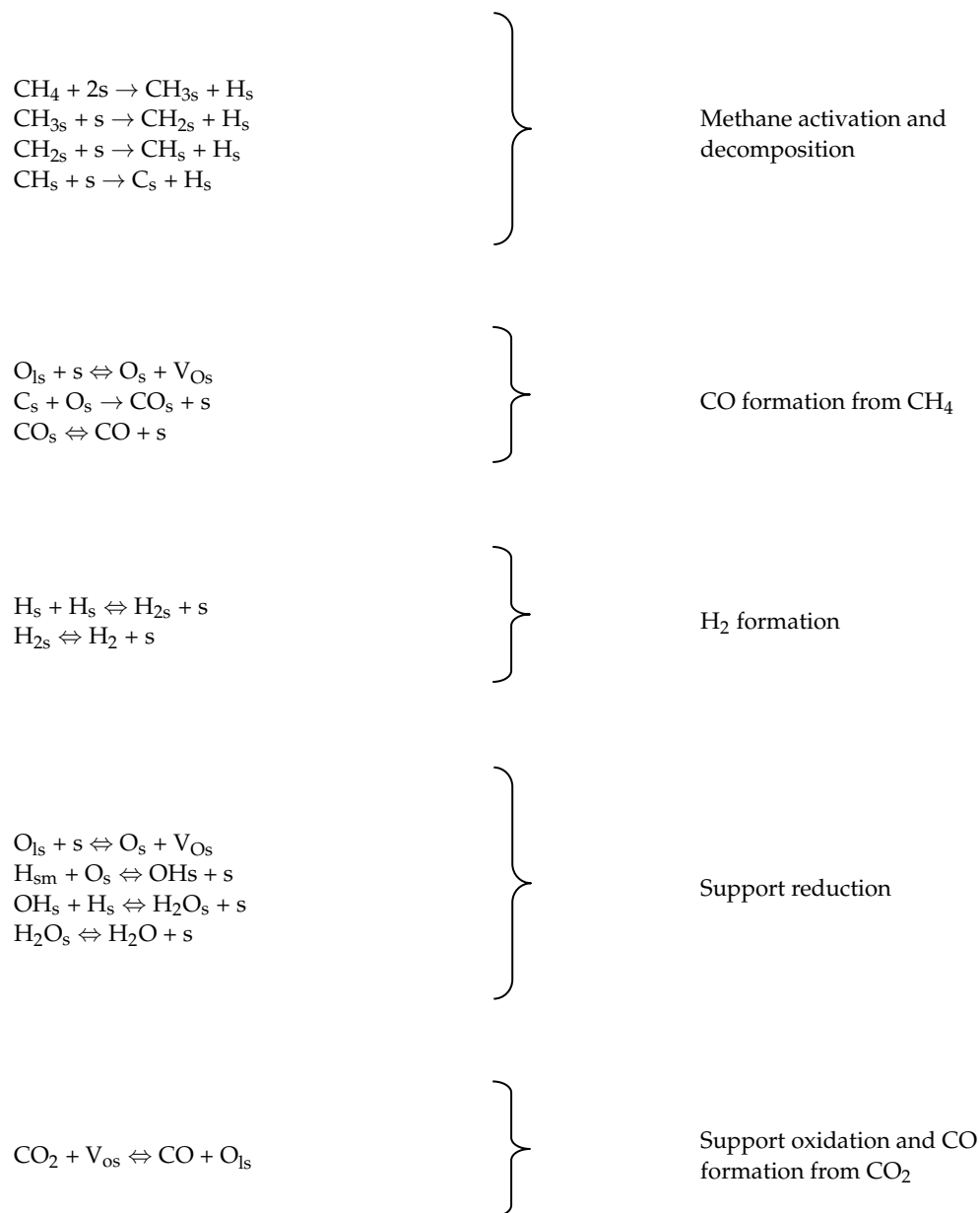
stability of Ni-loaded catalysts in fuels reforming, as expected, were obtained in the case of Mg-doped alumina [72,90,129,131,133] or $MgAl_2O_4$ [12,28,70,75,78–80,123,124,126,128,129].

In our studies [72,73,77,90,104,129], both Mg–γ-Al_2O_3 supports prepared by supporting Mg on γ-Al_2O_3 as well as mesoporous Mg–γ-Al_2O_3 and $MgAl_2O_4$ supports prepared by EISA method with Pluronic P123 were used. Ni was supported either by impregnation or during one-pot synthesis. Nanocomposite active components comprised of mixed oxides with perovskite, fluorite and spinel structures described above were supported by impregnation and then promoted by Ni+Ru. Catalysts were tested in dry reforming of methane and steam/autothermal reforming of ethanol as fractions as well as layers supported on small plates of heat-conducting substrates. Even for catalysts containing only Ni prepared by one-pot synthesis a high and stable performance in ethanol steam reforming was demonstrated due to a high dispersion of metal and acidity suppression [129]. The most promising active components comprised of mesoporous $MgAl_2O_4$ with supported $PrNi_{0.9}Ru_{0.1}O_3$, $MnCr_2O_4$ or $Ce_{0.35}Zr_{0.35}Pr_{0.3}O_3$ promoted with Ni+Ru demonstrated a high efficiency and resistance to coking in dry reforming of natural gas and autothermal reforming of such fuels as ethanol and ethyl acetate [78]. In a similar way, Ni/$CeZrO_2$/$MgAl_2O_4$ catalyst revealed a high activity and coking stability in tri-reforming of methane due to a small size of Ni nanoparticles and moderate basicity of support [28]. In steam reforming of methane [80] a high activity of Rh-Ni/$MgAl_2O_4$ washcoated FeCrAlloy honeycomb monolith was observed and explained by a high active metal dispersion as well as absence of heat and mass transfer limitations.

5. Mechanisms of Main Reactions

5.1. Partial Oxidation and Dry Reforming of Methane

Mechanism of these reactions was studied by using such methods as SSITKA, kinetic transients and pulse techniques (pulse microcalorimetry, pulse studies in flow conditions including those carried out in vacuum systems called TAP) [19,72,82,87,101,102,108,109,111,112,134–137]. For majority of efficient catalysts based on mixed oxides with a high mobility and storage capacity of reactive oxygen species with supported Pt group metals and/or Ni mechanism can be described by so called bifunctional type, where molecules of oxidants are activated on support vacancies producing oxygen species (and CO in the case of CO_2), while methane is activated on metal sites by C-H bond rupture (rate-limiting stage). These steps are conjugated by rapid transfer of surface oxygen species to the metal sites where they interact with CH_x fragment transforming them into CO and H_2. A typical feature of such redox scheme in the case of MDR is the same degree of methane conversion and syngas selectivity in pulses containing only CH_4 or CH_4 + CO_2, as well as identical CO_2 conversion into CO in mixed and CO_2—containing pulses. Simplified scheme of methane dry reforming and sequence of elementary steps successfully applied for modeling of transient over Ni-Ru-$Sm_{0.15}Pr_{0.15}Ce_{0.35}Zr_{0.35}O_2$ catalyst [72] are shown below:

$$CH_4 + 2s \rightarrow CH_{3s} + H_s$$
$$CH_{3s} + s \rightarrow CH_{2s} + H_s$$
$$CH_{2s} + s \rightarrow CH_s + H_s$$
$$CH_s + s \rightarrow C_s + H_s$$

Methane activation and decomposition

$$O_{ls} + s \Leftrightarrow O_s + V_{Os}$$
$$C_s + O_s \rightarrow CO_s + s$$
$$CO_s \Leftrightarrow CO + s$$

CO formation from CH_4

$$H_s + H_s \Leftrightarrow H_{2s} + s$$
$$H_{2s} \Leftrightarrow H_2 + s$$

H_2 formation

$$O_{ls} + s \Leftrightarrow O_s + V_{Os}$$
$$H_{sm} + O_s \Leftrightarrow OHs + s$$
$$OH_s + H_s \Leftrightarrow H_2O_s + s$$
$$H_2O_s \Leftrightarrow H_2O + s$$

Support reduction

$$CO_2 + V_{os} \Leftrightarrow CO + O_{ls}$$

Support oxidation and CO formation from CO_2

Here $\rightarrow$—denotes irreversible steps; $\Leftrightarrow$—reversible steps; s—surface sites; O_{ls}—lattice oxygen atoms; V_{Os}—lattice oxygen vacancy, sm—surface metal sites

For catalysts comprised of Pt/doped CeZrO oxides direct route of CH_4 partial oxidation into syngas, which generates CO and H_2 even in the presence of oxygen, was reliably demonstrated in our studies. It is explained by stabilization of Pt cations due to metal-support interaction and fast migration of oxygen species activated on support to Pt. Moreover, Pt cations are less efficient in oxidation of CO and H_2, while being more efficient in C-H bond activation in CH_4.

Basic scheme of methane partial oxidation [109] is presented here:

(1) $O_2 + 2Pt \Leftrightarrow 2PtO$
(2) $H_2O + z \Leftrightarrow H_2 + zO$
(3) $zO + Pt \Leftrightarrow PtO + z$ spillover
(4) $O_{bulk} + z \Leftrightarrow zO + V_O$ (bulk) diffusion
(5) $CH_4 + PtO \rightarrow CO + 2H_2 + Pt$
(6) $CH_4 + 4PtO \rightarrow CO_2 + 2H_2O + 4Pt$

(7) $CO + PtO \rightarrow CO_2 + Pt$

(8) $H_2 + PtO \rightarrow H_2O + Pt$

(9) $Pt + CO + H_2O \Leftrightarrow CO_2 + H_2 + Pt$

Clearly this mechanism is impossible in the case of such supported metals as Ru, Pd, Ni, Co, etc., which can only combust methane, CO and H_2 in the oxidized state. For these catalysts indirect scheme of methane partial oxidation is realized, in which all oxygen is consumed for methane combustion in the inlet part of the catalytic layer, while syngas is generated via steam and dry reforming of methane in the main part of catalytic layer where O_2 is absent in the gas phase and supported metals are in the reduced state [82].

These unique features of Pt cations were also reflected in specificity of MDR relaxation after contact of oxidized Pt/PrCeZrO catalyst with reaction feed, where both CH_4 and CO_2 conversions decline with time-on-stream apparently caused by the catalyst progressing reduction [19,136,137]. Mathematical modeling using scheme of methane dry reforming mechanism given below allowed to describe such transients taking into account a high efficiency of Pt cations in CH_4 activation, while CO_2 transformation occurs via carbonates adsorbed on Pt^{n+}–Pr^{4+}–O oxidized sites:

(1) $CO_2 + [PtO] \leftrightarrow [PtCO_3]$

(2) $CH_4 + [PtCO_3] \rightarrow 2\,CO + 2\,H_2 + [PtO]$

(3) $CH_4 + [PtO] \rightarrow CO + 2\,H_2 + [Pt]$

(4) $[Pt] + [O_s] \leftrightarrow [PtO] + [V_s]$

(5) $CO_2 + [V_s] \rightarrow CO + [O_s]$

(6) $H_2 + [PtO] \rightarrow H_2O + [Pt]$

Here [PtO] and [Pt] denote the oxidized and vacant Pt-centers, [PtCO$_3$] is the carbonate complex, [O$_s$] and [V$_s$] are the oxidized and vacant sites inside the lattice layer of Pt/PrSmCeZrO complex oxide composite,

Note that for catalysts with all other supported transition and precious metals in oxidized state catalytic activity in MDR is negligible and begins to increase to the steady-state value in the process of catalysts reduction by reaction mixture at sufficiently high temperatures.

### 5.2. Reactions of Ethanol Transformation into Syngas

For steady-state of catalysts based on oxides with high oxygen mobility and reactivity in ethanol reforming reactions pulse studies revealed that ethanol conversion and products selectivities in pulses containing reaction mixture or only ethanol are practically the same [103,104,121]. This proves realization of step-wise redox mechanism of these reactions. FTIRS studies combined with SSITKA identified main intermediates of ethanol conversion into syngas, such as ethoxy species and acetaldehyde and estimated rate constants of their transformation, while acetates were shown to be spectators. The rate-limiting step is the cleavage of C–C bond in ethoxy species fixed on rare-earth or transition metal cations due to incorporation of terminal oxygen species located on neighboring Me sites as supported by DFT calculations for the (001) face of $MnCr_2O_4$ spinel doped by Ru [104]. Kinetic scheme of the reaction of ethanol partial oxidation used in analysis of SSITKA data is as follows:

(1) $O_2 + 2[Z] \rightarrow 2\,[ZO]$

(2) $C_2H_5OH + [ZO] \rightarrow C_2H_4O + H_2O + [Z]$

(3) $C_2H_4O + (2+n)[ZO] \rightarrow CO + CO_2 + nH_2O + (2-n)H_2 + (2+n)[Z], n = 0\text{–}2$

(4) $CO + [ZO] \leftrightarrow CO_2 + [Z]$

(5) $H_2 + [ZO] \leftrightarrow H_2O + [Z]$

where [ZO] and [Z] correspond to oxidized and reduced site of catalysts surface, respectively, without any differentiation of the nature of active sites related to different transition metal cations (Mn, Cr) and metal atoms (Ni, Ru) at this level of analysis similar to that for catalysts based on bulk $MnCr_2O_4$ [104].

6. Development of Structured Catalysts

For design of such catalysts substrates made of metals, alloys and cermets were used [72,73,77,82,84,86,87,90,91,98,117]. Detonation spraying [138] was applied to cover thin foils, microchannel plates or gauzes by protective nonporous layer of alumina or zirconia. Known procedures of stacking and winding were applied to produce monolithic substrates from these constituents. Foam substrates comprised of NiAl alloys, ceramics, etc. were prepared via polyurethane foam duplication followed by required mechanical and thermal treatment [73,86]. These substrates were covered by catalytic layers using suspensions of active components in isopropanol. Structured catalysts were tested in pilot reactors in processes of natural gas, liquid fuels and biofuels reforming/autothermal reforming under realistic conditions. For best catalysts on substrates with a high thermal conductivity a high syngas yield was provided even at short contact times due to more uniform temperature profile along the catalysts' length [73,82,84]. In the autothermal reforming mode it helps to transfer heat generated in the inlet part of monolith due to exothermal combustion of a part of fuel into the following parts where O_2 in the gas phase is absent, so endothermic reactions of steam and dry reforming occur. For strongly endothermic reaction of MDR this positive effect of a high thermal conductivity of substrate is demonstrated by the identical temperature dependence of methane conversion in the layer of catalyst fraction for diluted feed and for the stack of microchannel plates with the same active component even in more concentrated feed (Figure 5b). In dry reforming of real natural gas (NG) containing up to 6% of C_2–C_4 alkanes also high and stable performance of structured catalyst was demonstrated for concentrated feed (Figure 6).
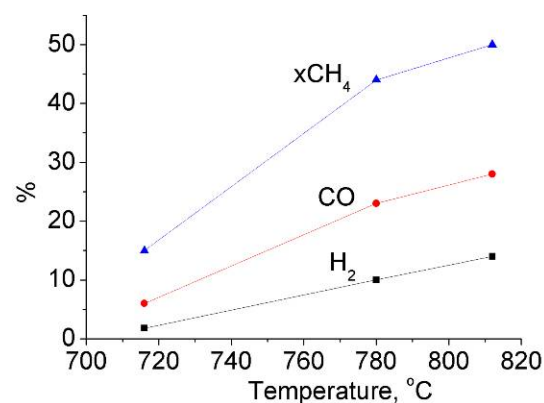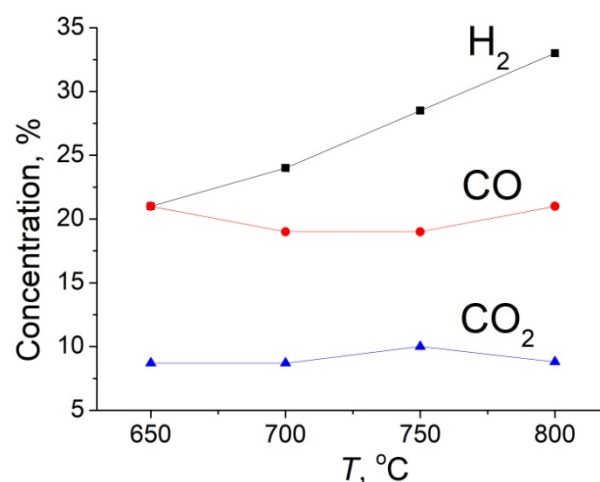
Figure 6. Temperature dependence of CH_4 conversion and CO/H_2 concentrations in NG dry reforming on the package of 5 Fechraloy microchannel plates with 1% NiO+1% Ru /SmPrCeZrO active component. Feed 50% CO_2 +40% NG +N_2, contact time 0.1 s.

This advantage of structured catalysts on heat-conducting metal/cermet substrates allowed to carry out efficient transformation of a lot of fuels including gasoline and diesel into syngas via partial oxidation and steam/autothermal reforming [82–87,117,139–142]. Reforming of biofuels such as acetone, ethyl acetate and glycerol is known to be accompanied by gas-phase reactions yielding ethylene, which is easily transformed into coke on catalysts. However, structured catalysts with nanocomposite active components demonstrated high and stable performance in the autothermal reforming of such biofuels as ethanol, acetone, ethyl acetate (Figure 7) and glycerol (Figure 8) with fuels content up to 25% and O_2 content in the mixture with steam up to 20% [73,82,86,87,117]. Note that Figures 7 and 8 show a high yield of syngas achieved at very short contact times, which is provided by a high efficiency of active components supported on mesoporous $MgAl_2O_4$ or Mg-doped −γ-Al_2O_3. Even anisole (content in the feed up to 10%), sunflower oil (content up to 0.7%) [82,117] and turpentine oil (commercial bio-oil mainly containing $C_{10}H_{16}$ and $C_{10}H_{18}O$ components, such as α-pinen, α-terpineol, etc., content in the feed up to 6% [90]) (Figure 9) were successfully converted into syngas in the autothermal reforming on de-

veloped structured catalysts. Another important problem in design of efficient syngas generators, especially for the small-scale application, is related to the heat management, since endothermic reactions of fuels steam and dry reforming require extensive preheat of inlet streams. This can be dealt with by using the exit stream for preheating the inlet feed in specially designed heat exchangers conjugated with catalytic reactors. Another aspect of energy efficiency problem solution is bound with possibility to conjugate exothermal partial oxidation of methane into syngas with endothermal processes of biofuels steam/dry reforming. These problems were solved in design of a radial-type reactor equipped with the heat exchanger described in detail in our previous work [82,117]. Here a cylindrical stack of catalytic microchannel washers was wrapped by gauze sheets with supported active components as well as with microspherical catalysts loaded between gauzes. The feed enters the central part of the stack of washers and flows in the radial direction. The reformed gas is collected into a plenum around the catalyst arrangement and exited from a single pipe, while inlet feed is heated by passing through the heat exchanger situated around the reactor as an outer shell. Such design made it possible to efficiently carry out partial oxidation of a mixture of natural gas and liquid fuel (ethanol, ethyl acetate, turpentine oil) to syngas at high flow rates (up to 40,000 h^{-1}) with preheating the mixture up to 50–100 °C at the reactor inlet (Figures 10–12).
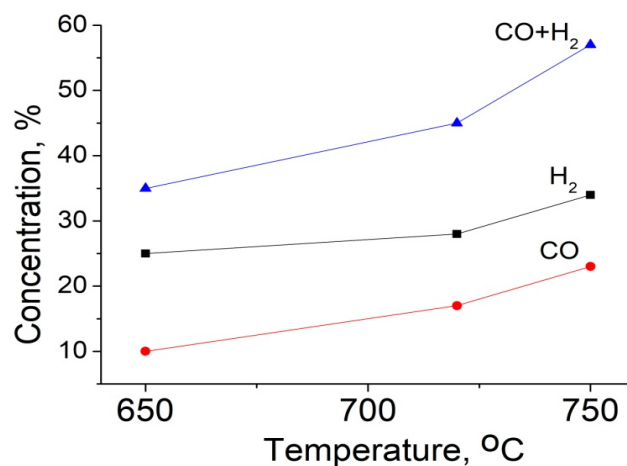
Figure 7. Temperature dependence of product concentrations in ATR of ethylacetate over the monolithic honeycomb catalyst comprised of FeCrAl gauzes loaded with NiRu/CeZrPrO on mesoporous MgAl$_2$O$_4$. Feed 30% EtAc + 60% H$_2$O + 8% O$_2$, N$_2$—balance, contact time 0.1 s.

Figure 8. Temperature dependence of products concentration in the process of glycerol autothermal reforming on microchannel CrAlO substrate with supported (Ni + Ru)/MnCr$_2$O$_4$/10% MgO–γ-Al$_2$O$_3$ active component. Feed 15% O$_2$ + 22% glycerol + 22% H$_2$O + N$_2$, contact time 0.06 s.
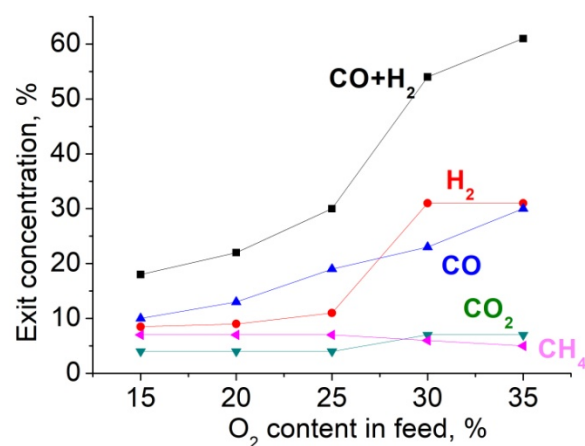
Figure 9. Dependence of products concentrations on oxygen content in the feed in the process of turpentine oil autothermal reforming on 3.4% LaNiPt/La–Ce–Zr–O/Fechraloy thin foil honeycomb at 800 °C. Feed 7% turpentine + 40% $H_2O+O_2+N_2$, contact time 0.5 s.
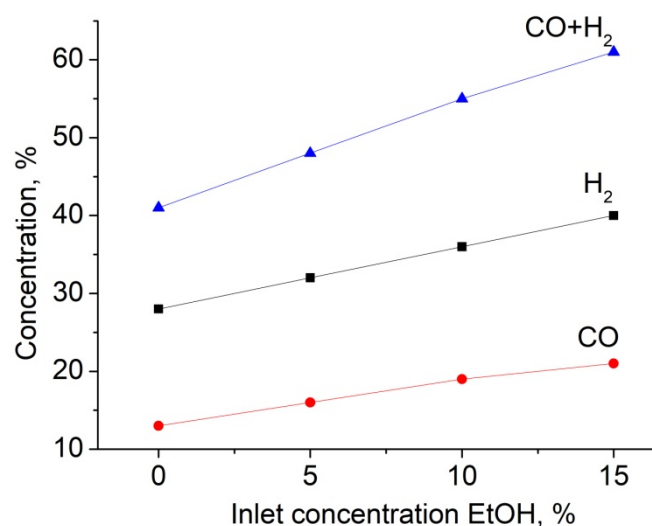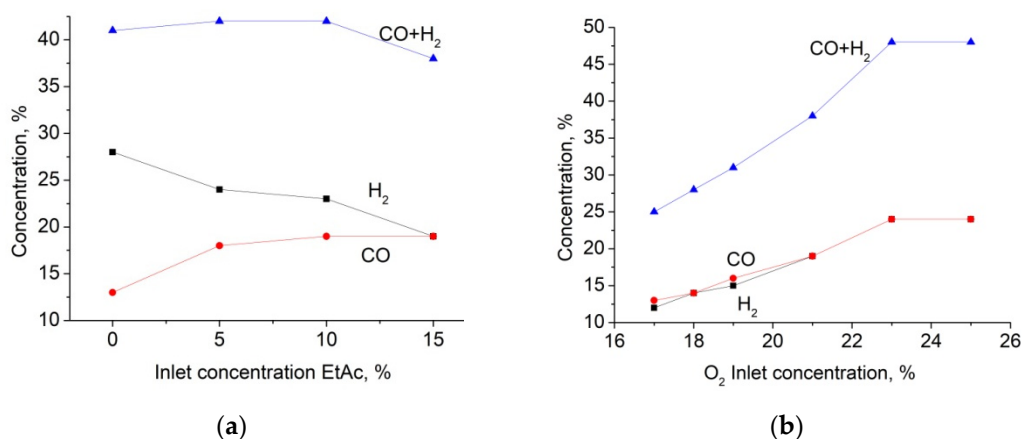

Figure 10. Dependence of products concentration on ethanol content in feed 24% NG + 16–25% O_2 + N_2 + EtOH in the process of autothermal reforming in the radial reactor with the heat exchanger. Flow rate 2.5 m^3/h, $LaNi(Pt)O_3/La_{0.1}Ce_{0.45}Zr_{0.45}O_2$ active component.

(**a**)   (**b**)

Figure 11. Dependence of products concentration on ethyl acetate (**a**) or O_2 (**b**) content in the autothermal reforming of the mixture of natural gas and ethyl acetate in radial reactor with the heat exchanger and $LaNi(Pt)O_3/La_{0.1}Ce_{0.45}Zr_{0.45}O_2$ active component. Feed 20% NG + 18% O_2 +N_2 +EtAc (**a**) or 10% NG + O_2 + N_2 + 15% EtAc (**b**), flow rate 2.5 m^3/h.
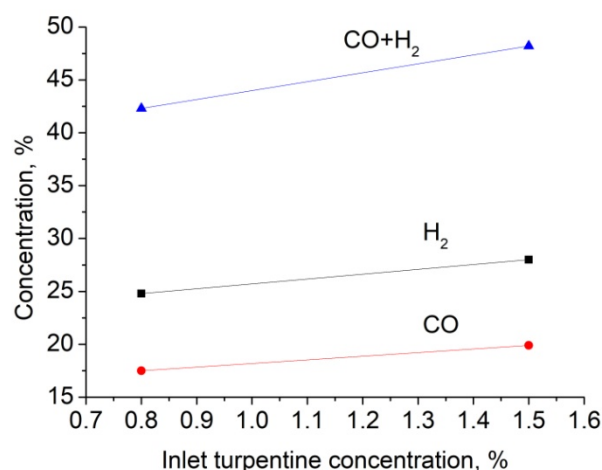
Figure 12. Dependence of products concentration on turpentine content in feed 20% NG +21% O_2 +N_2 +turpentine oil in the process of autothermal reforming in the radial reactor with the heat exchanger. Flow rate 2.5 m^3/h, LaNi(Pt)O$_3$/La$_{0.1}$Ce$_{0.45}$Zr$_{0.45}$O$_2$ active component.

7. Conclusions

Pechini method and synthesis in supercritical alcohols allowed to provide uniformity of the spatial distribution of elements in nanodomains of fluorite, perovskite and spinel oxides required for controlling their oxygen mobility and reactivity. Promoting these oxides and their nanocomposites of optimized composition by platinum group metals and nickel allowed to create effective and coking-resistant catalysts for biogas and biofuels transformation into syngas. Due to developed metal-support interface and strong metal–support interactions bifunctional scheme of reaction mechanism is realized with activation of oxidants (O_2, CO_2, H_2O) on the oxide support sites, while fuel molecules are activated on metal centers. Fast diffusion of surface oxygen species to the metal–oxide interface provides conjugation of these steps resulting in efficient syngas generation and coking suppression. Preparation of mesoporous supports comprised of MgAl$_2$O$_4$ or Mg-doped alumina with enhanced basicity allowed to design core-shell systems with a high working area of supported catalytic nanocomposite layers, increase their activity, thermal and coking stability and decrease content of rare-earth elements. Structured heat-conducting substrates loaded with optimized active components provide efficient heat- and mass-transfer in reactors for biofuels transformation into syngas. Pilot reactors with internal heat exchangers permit efficient operation in the autothermal mode on the mixture of natural gas, air and real biofuels such as ethanol, glycerol and turpentine oil with the inlet temperature 50–100°C and GHSV up to 40,000 h^{-1}.

Author Contributions: Writing—original draft preparation, V.S., N.E., M.S. and N.M.; writing—review and editing, V.S. All authors have read and agreed to the published version of the manuscript.

Institutional Review Board Statement: Not applicable.

Informed Consent Statement: Not applicable.

Conflicts of Interest: The authors declare no conflict of interest.

References

1. Bepari, S.; Kuila, D. Steam reforming of methanol ethanol and glycerol over nickel-based catalysts—A review. *Int. J. Hydrogen Energy* **2020**, *45*, 18090–18113. [CrossRef]
2. Chattahathan, S.A.; Adhikari, A.; Abdoulmoumine, N. A review on current status of hydrogen production from bio-oil. *Renew. Sustain. Energy Rev.* **2012**, *16*, 2366–2372. [CrossRef]
3. Aziz, M.A.A.; Setiabudi, H.D.; Teh, L.P.; Annuar, N.H.R.; Jalil, A.A. A review of heterogeneous catalysts for syngas production via dry reforming. *J. Taiwan Inst. Chem. Eng.* **2019**, *101*, 139–158. [CrossRef]
4. Chen, J.; Sun, J.; Wang, Y. Catalysts for steam reforming of bio-oil: A review. *Ind. Eng. Chem. Res.* **2016**, *56*, 4627–4637. [CrossRef]
5. Dou, B.; Song, Y.; Wang, C.; Chen, H.; Xu, Y. Hydrogen production from catalytic steam reforming of biodiesel byproduct glycerol: Issues and challenges. *Renew. Sustain. Energy Rev.* **2014**, *30*, 950–960. [CrossRef]
6. Anil, C.; Modak, J.M.; Madras, G. Syngas production via CO_2 reforming of methane over noble metal (Ru, Pt, and Pd) doped $LaAlO_3$ perovskite catalyst. *Mol. Catal.* **2020**, *484*, 110805. [CrossRef]
7. Pakhare, D.; Spivey, J. A review of dry (CO_2) reforming of methane over noble metal catalysts. *Chem. Soc. Rev.* **2014**, *43*, 7813–7837. [CrossRef] [PubMed]
8. Yentekakis, I.V.; Panagiotopoulou, P.; Artemakis, G. A review of recent efforts to promote dry reforming of methane (DRM) to syngas production via bimetallic catalyst formulations. *Appl. Catal. B Environ.* **2021**, *296*, 120210. [CrossRef]
9. Bae, J.; Lee, S.; Kim, S.; Oh, J.; Choi, S.; Bae, M.; Kang, I.; Katikaneni, S.P. Liquid fuel processing for hydrogen production: A review. *Int. J. Hydrogen Energy* **2016**, *41*, 19990–20022. [CrossRef]
10. Pham, T.T.P.; Ro, K.S.; Chen, L.; Mahajan, D.; Siang, T.J.; Ashik, U.P.M.; Hayashi, J.; Minh, D.H.; Vo, D.-V.N. Microwave-assisted dry reforming of methane for syngas production: A review. *Environ. Chem. Lett.* **2020**, *18*, 1987–2019. [CrossRef]
11. Gao, X.; Ashok, J.; Kawi, S. Smart designs of anti-coking and anti-sintering Ni-based catalysts for dry reforming of methane: A recent review. *Reactions* **2020**, *1*, 162–194. [CrossRef]
12. Cho, E.; Lee, Y.-H.; Kim, H.; Jang, E.J.; Kwak, J.H.; Lee, K.; Ko, C.H.; Yoon, W.L. Ni catalysts for dry methane reforming prepared by A-site exsolution on mesoporous defect spinel magnesium aluminate. *Appl. Catal. A Gen.* **2020**, *602*, 117694. [CrossRef]
13. Sadykov, V.A.; Kuznetsova, T.G.; Alikina, G.M.; Frolova, Y.V.; Lukashevich, A.I.; Muzykantov, V.S.; Rogov, V.A.; Batuev, L.C.; Kriventsov, V.V.; Kochubei, D.I.; et al. Ceria-based fluorite-like oxide solid solutions promoted by precious metals as catalysts of methane transformation into syngas. In *New Topics in Catalysis Research*; McReynolds, D.K., Ed.; Nova Science Publishers: Hauppauge, NY, USA, 2007; pp. 97–196.
14. Charisiou, N.D.; Iordanidis, A.; Polychronopoulou, K.; Yentekakis, I.V.; Goula, M.A. Studying the stability of Ni supported on modified with CeO_2 alumina catalysts for the biogas dry reforming reaction. *Mater. Today Proc.* **2018**, *5*, 27607–27616. [CrossRef]
15. Faria, E.C.; Neto, R.C.R.; Colman, R.C.; Noronha, F.B. Hydrogen production through CO_2 reforming of methane over $Ni/CeZrO_2/Al_2O_3$ catalysts. *Catal. Today* **2014**, *228*, 138–144. [CrossRef]
16. Grabchenko, M.; Pantaleo, G.; Puleo, F.; Kharlamova, T.S.; Zaikovskii, V.I.; Vodyankina, O.; Liotta, L.F. Design of Ni based catalysts supported over binary La-Ce oxides: Influence of La/Ce ratio on the catalytic performances in DRM. *Catal. Today* **2021**. [CrossRef]
17. Vagia, E.C.; Lemonidou, A.A. Investigations on the properties of ceria–zirconia-supported Ni and Rh catalysts and their performance in acetic acid steam reforming. *J. Catal.* **2010**, *269*, 388–396. [CrossRef]
18. Sadykov, V.A.; Kuznetsova, T.G.; Frolova, Y.V.; Alikina, G.M.; Lukashevich, A.I.; Rogov, V.A.; Muzykantov, V.S.; Pinaeva, L.G.; Sadovskaya, E.M.; Ivanova, Y.A.; et al. Fuel-rich methane combustion: Role of the Pt dispersion and oxygen mobility in a fluorite-like complex oxide support. *Catal. Today* **2006**, *117*, 475–483. [CrossRef]
19. Mirodatos, C.; van Veen, A.C.; Pokrovskaya, S.A.; Chumakova, N.A.; Sazonova, N.N.; Sadykov, V.A. Modeling of transient studies on the reaction kinetics over catalysts with lattice oxygen mobility: Dry reforming of CH_4 over a Pt/PrCeZrO catalyst. *Chem. Eng. J.* **2018**, *343*, 530–543. [CrossRef]
20. Smirnova, M.Y.; Pavlova, S.N.; Krieger, T.A.; Bespalko, Y.N.; Anikeev, V.I.; Chesalov, Y.A.; Kaichev, V.V.; Mezentseva, N.V.; Sadykov, V.A. The synthesis of $Ce_{1-x}Zr_xO_2$ oxides in supercritical alcohols and catalysts for carbon dioxide reforming of methane on their basis. *Russ. J. Phys. Chem. B* **2017**, *11*, 1–10. [CrossRef]
21. Simonov, M.; Bespalko, Y.; Smal, E.; Valeev, K.; Fedorova, V.; Krieger, T.; Sadykov, V. Nickel-containing ceria-zirconia doped with Ti and Nb. Effect of support composition and preparation method on catalytic activity in methane dry reforming. *Nanomaterials* **2020**, *10*, 1281. [CrossRef] [PubMed]
22. Bespalko, Y.; Smal, E.; Simonov, M.; Valeev, K.; Fedorova, V.; Krieger, T.; Cherepanova, S.; Ishchenko, A.; Rogov, V.; Sadykov, V. Novel $Ni/Ce(Ti)ZrO_2$ catalysts for methane dry reforming prepared in supercritical alcohol media. *Energies* **2020**, *13*, 3365. [CrossRef]
23. Pavlova, S.; Smirnova, M.; Bobin, A.; Cherepanova, S.; Kaichev, V.; Ishchenko, A.; Selivanova, A.; Rogov, V.; Roger, A.-C.; Sadykov, V. Structural, textural, and catalytic properties of $Ni-Ce_xZr_{1-x}O_2$ catalysts for methane dry reforming prepared by continuous synthesis in supercritical isopropanol. *Energies* **2020**, *13*, 3728. [CrossRef]
24. Fedorova, V.; Simonov, M.; Valeev, K.; Bespalko, Y.; Smal, E.; Eremeev, N.; Sadovskaya, E.; Krieger, T.; Ishchenko, A.; Sadykov, V. Kinetic regularities of methane dry reforming reaction on nickel-containing modified ceria-zirconia. *Energies* **2021**, *14*, 2973. [CrossRef]

25. Auxéméry, A.; Frias, B.B.; Smal, E.; Dziadek, K.; Philippot, G.; Legutko, P.; Simonov, M.; Thomas, S.; Adamski, A.; Sadykov, V.; et al. Continuous supercritical solvothermal preparation of nanostructured ceria-zirconia as supports for dry methane reforming catalysts. *J. Supercrit. Fluids* **2020**, *162*, 104855. [CrossRef]

26. Smirnova, M.Y.; Bobin, A.S.; Pavlova, S.N.; Ishchenko, A.V.; Selivanova, A.V.; Kaichev, V.V.; Cherepanova, S.V.; Krieger, T.A.; Arapova, M.V.; Roger, A.-C.; et al. Methane dry reforming over Ni catalysts supported on Ce–Zr oxides prepared by a route involving supercritical fluids. *Open Chem.* **2017**, *15*, 412–425. [CrossRef]

27. Kambolis, A.; Matralis, H.; Trovarelli, A.; Papadopoulou, C.H. Ni/CeO$_2$-ZrO$_2$ catalysts for the dry reforming of methane. *Appl. Catal. A Gen.* **2010**, *377*, 16–26. [CrossRef]

28. Lino, A.V.P.; Rodella, C.B.; Assaf, E.M.; Assaf, J.M. Methane tri-reforming for synthesis gas production using Ni/CeZrO$_2$/MgAl$_2$O$_4$ catalysts: Effect of Zr/Ce molar ratio. *Int. J. Hydrogen Energy* **2020**, *45*, 8418–8432. [CrossRef]

29. Shoynkhorova, T.B.; Simonov, P.A.; Potemkin, D.I.; Snytnikov, P.V.; Belyaev, V.D.; Ishchenko, A.V.; Svintsitskiy, D.A.; Sobyanin, V.A. Highly dispersed Rh-, Pt-, Ru/Ce$_{0.75}$Zr$_{0.25}$O$_{2-\delta}$ catalysts prepared by sorption-hydrolytic deposition for diesel fuel reforming to syngas. *Appl. Catal. B Environ.* **2018**, *237*, 237–244. [CrossRef]

30. Shahnazi, A.; Firoozi, S. Improving the catalytic performance of LaNiO$_3$ perovskite by manganese substitution via ultrasonic spray pyrolysis for dry reforming of methane. *J. CO$_2$ Util.* **2021**, *45*, 101455. [CrossRef]

31. Naurzkulova, S.M.; Arapova, M.V.; Ishchenko, A.V.; Krieger, T.A.; Saraev, A.A.; Kaichev, V.V.; Rogov, V.A.; Krasnov, A.V.; Massalimova, B.K.; Sadykov, V.A. Ni–Ru-containing mixed oxide-based composites as precursors for ethanol steam reforming catalysts: Effect of the synthesis methods on the structural and catalytic properties. *Open Chem.* **2021**, *19*, 696–708. [CrossRef]

32. Sadykov, V.A.; Pavlova, S.N.; Alikina, G.M.; Sazonova, N.N.; Mezentseva, N.V.; Arapova, M.V.; Rogov, V.A.; Krieger, T.A.; Ishhenko, A.V.; Gulyaev, R.V.; et al. Perovskite-based catalysts for transformation of natural gas and oxygenates into syngas. In *Perovskite: Crystallography, Chemistry and Catalytic Performance*; Zhang, J., Li, H., Eds.; Nova Science Publishers: Hauppauge, NY, USA, 2013; pp. 1–58.

33. Barros, B.S.; Melo, D.M.A.; Libs, S.; Kiennemann, A. CO$_2$ reforming of methane over La$_2$NiO$_4$/α-Al$_2$O$_3$ prepared by microwave assisted self-combustion method. *Appl. Catal. A Gen.* **2010**, *378*, 69–75. [CrossRef]

34. Pavlova, S.; Kapokova, L.; Bunina, R.; Alikina, G.; Sazonova, N.; Krieger, T.; Ishchenko, A.; Rogov, V.; Gulyaev, R.; Sadykov, V.; et al. Syngas production by CO$_2$ reforming of methane using LnFeNi(Ru)O$_3$ perovskites as precursors of robust catalysts. *Catal. Sci. Technol.* **2012**, *2*, 2099–2108. [CrossRef]

35. Sadykov, V.A.; Pavlova, S.N.; Kharlamova, T.S.; Muzykantov, V.S.; Uvarov, N.F.; Okhlupin, Y.S.; Ishchenko, A.V.; Bobin, A.S.; Mezentseva, N.V.; Alikina, G.M.; et al. Perovskites and their nanocomposites with fluorite-like oxides as materials for solid oxide fuel cells cathodes and oxygen-conducting membranes: Mobility and reactivity of the surface/bulk oxygen as a key factor of their performance. In *Perovskites: Structure, Properties and Uses*; Borowski, M., Ed.; Nova Science Publishers: Hauppauge, NY, USA, 2010; pp. 67–178.

36. Goldwasser, M.R.; Rivas, M.E.; Pietri, E.; Pérez-Zurita, M.J.; Cubeiro, M.L.; Grivobal-Constant, A.; Leclercq, G. Perovskites as catalysts precursors: Synthesis and characterization. *J. Mol. Catal. A Chem.* **2005**, *228*, 325–331. [CrossRef]

37. Tanaka, H.; Misono, M. Advances in designing perovskite catalysts. *Curr. Opin. Solid State Mater. Sci.* **2001**, *5*, 381–387. [CrossRef]

38. Goldwasser, M.R.; Rivas, M.E.; Pietri, E.; Pérez-Zurita, M.J.; Cubeiro, M.L.; Gingembre, L.; Leclercq, L.; Leclercq, G. Perovskites as catalysts precursors: CO$_2$ reforming of CH$_4$ on Ln$_{1-x}$Ca$_x$Ru$_{0.8}$Ni$_{0.2}$O$_3$ (Ln = La, Sm, Nd). *Appl. Catal. A Gen.* **2003**, *255*, 45–57. [CrossRef]

39. Bhattar, D.; Abedin, M.A.; Kanitkar, S.; Spivey, J.J. A review on dry reforming of methane over perovskite derived catalysts. *Catal. Today* **2021**, *365*, 2–23. [CrossRef]

40. Mawdsley, J.R.; Krause, T.R. Rare earth-first-row transition metal perovskites as catalysts for the autothermal reforming of hydrocarbon fuels to generate hydrogen. *Appl. Catal. A Gen.* **2008**, *334*, 311–320. [CrossRef]

41. Batiot-Dupeyrat, C.; Gallego, G.A.S.; Mondragon, F.; Barrault, J.; Tatibouët, J.-M. CO$_2$ reforming of methane over LaNiO$_3$ as precursor material. *Catal. Today* **2005**, *107–108*, 474–480. [CrossRef]

42. Pereniguez, R.; Gonzalez-DelaCruz, V.M.; Holgado, J.P.; Caballero, A. Synthesis and characterization of a LaNiO$_3$ perovskite as precursor for methane reforming reactions catalysts. *Appl. Catal. B Environ.* **2010**, *93*, 346–353. [CrossRef]

43. Moradi, G.R.; Rahmanzade, M.; Sharifni, S. Kinetic investigation of CO$_2$ reforming of CH$_4$ over La–Ni based perovskite. *Chem. Eng. J.* **2010**, *162*, 787–791. [CrossRef]

44. Nam, J.W.; Chae, H.; Lee, S.H.; Jung, H.; Lee, K.-Y. Methane dry reforming over well-dispersed Ni catalyst prepared from perovskite-type mixed oxides. *Stud. Surf. Sci. Catal.* **1998**, *119*, 843–848.

45. Valderrama, G.; Goldwasser, M.R.; Urbina de Navarro, C.; Tatibouët, J.M.; Barrault, J.; Batiot-Dupeyrat, C.; Martınez, F. Dry reforming of methane over Ni perovskite type oxides. *Catal. Today* **2005**, *107–108*, 785–791. [CrossRef]

46. Rynkowski, J.; Samulkiewicz, P.; Ladavos, A.K.; Pomonis, P.J. Catalytic performance of reduced La$_{2-x}$Sr$_x$NiO$_4$ perovskite-like oxides for CO$_2$ reforming of CH$_4$. *Appl. Catal. A Gen.* **2004**, *263*, 1–9. [CrossRef]

47. Chettapongsaphan, C.; Charojrochkul, S.; Assabumrungrat, S.; Laosiripojana, N. Catalytic H$_2$O and CO$_2$ reforming of CH$_4$ over perovskite-based La$_{0.8}$Sr$_{0.2}$Cr$_{0.9}$Ni$_{0.1}$O$_3$: Effects of pre-treatment and co-reactant/CH$_4$ on its reforming characteristics. *Appl. Catal. A Gen.* **2010**, *386*, 194–200. [CrossRef]

48. Valderrama, G.; Kiennemann, A.; Goldwasser, M.R. La-Sr-Ni-Co-O based perovskite-type solid solutions as catalyst precursors in the CO$_2$ reforming of methane. *J. Power Sources* **2010**, *195*, 1765–1771. [CrossRef]

49. Mota, N.; Álvarez-Galván, M.C.; Al-Zahrani, S.M.; Navarro, R.M.; Fierro, J.L.G. Diesel fuel reforming over catalysts derived from LaCo$_{1-x}$Ru$_x$O$_3$ perovskites with high Ru loading. *Int. J. Hydrogen Energy* **2012**, *37*, 7056–7066. [CrossRef]

50. Gallego, G.S.; Batiot-Dupeyrat, C.; Barrault, J.; Florez, E.; Mondragon, F. Dry reforming of methane over LaNi$_{1-y}$By O$_{3\pm\delta}$ (B = Mg, Co) perovskites used as catalyst precursor. *Appl. Catal. A Gen.* **2008**, *334*, 251–258. [CrossRef]

51. Valderrama, G.; Kienneman, A.; Goldwasser, M.R. Dry reforming of CH$_4$ over solid solutions of LaNi$_{1-x}$Co$_x$O$_3$. *Catal. Today* **2008**, *133*, 142–148. [CrossRef]

52. Goldwasser, M.R.; Rivas, M.E.; Lugo, M.L.; Pietri, E.; Perez-Zurita, J.; Cubeiro, M.L.; Griboval-Constant, A.; Leclercq, G. Combined methane reforming in presence of CO$_2$ and O$_2$ over LaFe$_{1-x}$Co$_x$O$_3$ mixed-oxide perovskites as catalysts precursors. *Catal. Today* **2005**, *107–108*, 106–113. [CrossRef]

53. Bian, Z.; Wang, Z.; Jiang, B.; Hongmanorom, P.; Zhong, W.; Kawi, S. A review on perovskite catalysts for reforming of methane to hydrogen production. *Renew. Sustain. Energy Rev.* **2020**, *134*, 110291. [CrossRef]

54. Provendier, H.; Petit, C.; Estournes, C.; Kiennemann, A. Steam reforming of methane on LaNi$_x$Fe$_{1-x}$O$_3$ (0≤x≤1) perovskites. Reactivity and characterization after test. *C. R. Acad. Sci.—Ser. IIC—Chem.* **2001**, *4*, 57–66.

55. Provendier, H.; Petit, C.; Estournes, C.; Libs, S.; Kiennemann, A. Stabilization of active nickel catalysts in partial oxidation of methane to synthesis gas by iron addition. *Appl. Catal. A Gen.* **1999**, *180*, 163–173. [CrossRef]

56. Kapokova, L.; Pavlova, S.; Bunina, R.; Alikina, G.; Krieger, T.; Ishchenko, A.; Rogov, V.; Sadykov, V. Dry reforming of methane over LnFe$_{0.7}$Ni$_{0.3}$O$_{3-\delta}$ perovskites: Influence of Ln nature. *Catal. Today* **2011**, *164*, 227–233. [CrossRef]

57. Kim, W.Y.; Jang, J.S.; Ra, E.C.; Kim, K.Y.; Kim, E.H.; Lee, J.S. Reduced perovskite LaNiO$_3$ catalysts modified with Co and Mn for low coke formation in dry reforming of methane. *Appl. Catal. A Gen.* **2019**, *575*, 198–203. [CrossRef]

58. Gallego, G.S.; Marín, J.G.; Batiot-Dupeyrat, C.; Barrault, J.; Mondragon, F. Influence of Pr and Ce in dry methane reforming catalysts produced from La$_{1-x}$A$_x$NiO$_{3-\delta}$ perovskites. *Appl. Catal. A Gen.* **2009**, *369*, 97–103. [CrossRef]

59. Rivas, M.E.; Fierro, J.L.G.; Goldwasser, M.R.; Pietri, E.; Pérez-Zurita, M.J.; Griboval-Constant, A.; Lecler, G. Structural features and performance of LaNi$_{1-x}$Rh$_x$O$_3$ system for the dry reforming of methane. *Appl. Catal. A Gen.* **2008**, *344*, 10–19. [CrossRef]

60. Araujo, G.C.; Lima, S.M.; Assaf, J.M.; Pena, M.A.; Fierro, J.L.G.; Rangel, M.D.C. Catalytic evaluation of perovskite-type oxide LaNi$_{1-x}$Ru$_x$O$_3$ in methane dry reforming. *Catal. Today* **2008**, *133–135*, 129–135. [CrossRef]

61. Mota, N.; Alvarez-Galvána, M.C.; Navarro, R.M.; Al-Zahrani, S.M.; Goguet, A.; Daly, H.; Zhang, W.; Trunschke, A.; Schlögl, R.; Fierro, J.L.G. Insights on the role of Ru substitution in the properties of LaCoO$_3$-based oxides as catalysts precursors for the oxidative reforming of diesel fuel. *Appl. Catal. B Environ.* **2012**, *113–114*, 271–280. [CrossRef]

62. Chen, H.; Yu, H.; Peng, F.; Yang, G.; Wang, H.; Yang, J.; Tang, Y. Autothermal reforming of ethanol for hydrogen production over perovskite LaNiO$_3$. *Chem. Eng. J.* **2010**, *160*, 333–339. [CrossRef]

63. Liu, J.Y.; Lee, C.C.; Wang, C.H.; Yeh, C.T.; Wang, C.B. Application of nickel–lanthanum composite oxide on the steam reforming of ethanol to produce hydrogen. *Int. J. Hydrogen Energy* **2010**, *35*, 4069–4075. [CrossRef]

64. De Lima, S.M.; da Silva, A.M.; da Costa, L.O.O.; Assaf, J.M.; Jacobs, G.; Davis, B.H.; Mattos, L.V.; Noronha, F.B. Evaluation of the performance of Ni/La$_2$O$_3$ catalyst prepared from LaNiO$_3$ perovskite-type oxides for the production of hydrogen through steam reforming and oxidative steam reforming of ethanol. *Appl. Catal. A Gen.* **2010**, *377*, 181–190. [CrossRef]

65. Chen, S.Q.; Wang, H.; Liu, Y. Perovskite La–St–Fe–O (St = Ca, Sr) supported nickel catalysts for steam reforming of ethanol: The effect of the A site substitution. *Int. J. Hydrogen Energy* **2009**, *34*, 7995–8005. [CrossRef]

66. Chen, S.Q.; Li, Y.D.; Liu, Y.; Bai, X. Regenerable and durable catalyst for hydrogen production from ethanol steam reforming. *Int. J. Hydrogen Energy* **2011**, *36*, 5849–5856. [CrossRef]

67. De Lima, S.M.; da Silva, A.M.; da Costa, L.O.O.; Assaf, J.M.; Mattos, L.V.; Sarkari, R.; Venugopale, A.; Noronha, F.B. Hydrogen production through oxidative steam reforming of ethanol over Ni-based catalysts derived from La$_{1-x}$Ce$_x$NiO$_3$ perovskite-type oxides. *Appl. Catal. B Environ.* **2012**, *121–122*, 1–9. [CrossRef]

68. Sadovskaya, E.M.; Frolov, D.D.; Goncharov, V.B.; Fedorova, A.A.; Morozov, I.V.; Klyushin, A.Y.; Vinogradov, A.S.; Smal, E.A.; Sadykov, V.A. Mixed spinel-type Ni-Co-Mn oxides: Synthesis, structure and catalytic properties. *Catal. Sustain. Energy* **2016**, *3*, 25–31. [CrossRef]

69. Smal, E.A.; Simonov, M.N.; Mezentseva, N.V.; Krieger, T.A.; Larina, T.V.; Saraev, A.A.; Glazneva, T.S.; Ishchenko, A.V.; Rogov, V.A.; Eremeev, N.F.; et al. Spinel-type Mn$_x$Cr$_{3-x}$O$_4$-based catalysts for ethanol steam reforming. *Appl. Catal. B Environ.* **2021**, *283*, 119656. [CrossRef]

70. Medeiros, R.L.B.A.; Macedo, H.P.; Melo, V.R.M.; Oliveira, A.A.S.; Barros, J.M.F.; Melo, M.A.F.; Melo, D.M.A. Ni supported on Fe-doped MgAl$_2$O$_4$ for dry reforming of methane: Use of factorial design to optimize H$_2$ yield. *Int. J. Hydrogen Energy* **2016**, *41*, 14047–14057. [CrossRef]

71. Pinaeva, L.G.; Sadovskaya, E.M.; Smal, E.A.; Bobin, A.S.; Sadykov, V.A. Mechanism and kinetics of ethanol oxidation over Ru(Pt) supported onto Mn-Cr-O mixed oxides. *Chem. Eng. J.* **2018**, *333*, 101–110. [CrossRef]

72. Sadykov, V.A.; Bobrova, L.N.; Mezentseva, N.V.; Pavlova, S.N.; Fedorova, Y.E.; Bobin, A.S.; Vostrikov, Z.Y.; Glazneva, T.S.; Smirnova, M.; Sazonova, N.N.; et al. Methane dry reforming on nanocomposite catalysts: Design, kinetics and mechanism. In *Small-Scale Gas to Liquid Fuel Synthesis*; Kannelopoulos, N., Ed.; CRC Press, Taylor & Francis Group: Boca Raton, FL, USA, 2015; pp. 315–376.

73. Sadykov, V.; Mezentseva, N.; Simonov, M.; Smal, E.; Arapova, M.; Pavlova, S.; Fedorova, Y.; Chub, O.; Bobrova, L.; Kuzmin, V.; et al. Structured nanocomposite catalysts of biofuels transformation into syngas and hydrogen: Design and performance. *Int. J. Hydrogen Energy* **2015**, *40*, 7511–7522. [CrossRef]

74. Korneeva, E.V.; Kardash, T.Y.; Rogov, V.A.; Smal, E.A.; Sadykov, V.A. Catalytic steam reforming of ethanol over W-, V-, or Nb–modified Ni-Al-O hydrotalcite-type precursors. *Catal. Sustain. Energy* **2017**, *4*, 17–24. [CrossRef]

75. Hadian, N.; Rezaei, M. Combination of dry reforming and partial oxidation of methane over Ni catalysts supported on nanocrystalline $MgAl_2O_4$. *Fuel* **2013**, *113*, 571–579. [CrossRef]

76. Bian, Z.; Das, S.; Wai, M.H.; Hongmanorom, P.; Kawi, S. A review on bimetallic nickel-based catalysts for CO_2 reforming of methane. *ChemPhysChem* **2017**, *18*, 3117–3134. [CrossRef] [PubMed]

77. Sadykov, V.; Mezentseva, N.; Alikina, G.; Bunina, R.; Pelipenko, V.; Lukashevich, A.; Vostrikov, Z.; Rogov, V.; Krieger, T.; Ishchenko, A.; et al. Nanocomposite catalysts for steam reforming of methane and biofuels: Design and performance. In *Advances in Nanocomposites—Synthesis, Characterization and Industrial Applications*; Reddy, B., Ed.; INTECH: Vienna, Austria, 2011; pp. 909–946.

78. Sadykov, V.; Pavlova, S.; Fedorova, J.; Bobin, A.; Fedorova, V.; Simonov, M.; Ishchenko, A.; Krieger, T.; Melgunov, M.; Glazneva, T.; et al. Structured catalysts with mesoporous nanocomposite active components loaded on heat-conducting substrates for transformation of biogas/biofuels into syngas. *Catal. Today* **2021**, *379*, 166–180. [CrossRef]

79. Wysocka, J.H.I.; Rogala, A. Catalytic activity of nickel and ruthenium–nickel catalysts supported on SiO_2, ZrO_2, Al_2O_3, and $MgAl_2O_4$ in a dry reforming process. *Catalysts* **2019**, *9*, 540. [CrossRef]

80. Katheria, S.; Deo, G.; Kunzru, D. Rh-Ni/$MgAl_2O_4$ catalyst for steam reforming of methane: Effect of Rh doping, calcination temperature and its application on metal monoliths. *Appl. Catal. A Gen.* **2019**, *570*, 308–318. [CrossRef]

81. Lino, A.V.P.; Assaf, E.M.; Assaf, J.M. Adjusting process variables in methane tri-reforming to achieve suitable syngas quality and low coke deposition. *Energy Fuels* **2020**, *34*, 16522–16531. [CrossRef]

82. Sadykov, V.; Bobrova, L.; Pavlova, S.; Simagina, V.; Makarshin, L.; Parmon, V.; Ross, J.R.H.; Van Veen, A.C.; Mirodatos, C. *Syngas Generation from Hydrocarbons and Oxygenates with Structured Catalysts*; Nova Science Publishers: Hauppauge, NY, USA, 2012; p. 140.

83. Deutschman, O. Catalytic reforming of logistic fuels at high-temperatures. *Catalysis* **2012**, *24*, 48–82.

84. Bobrova, L.N.; Sadykov, V.A.; Mezentseva, N.V.; Pelipenko, V.V.; Vernikovskaya, N.V.; Klenov, O.P.; Smorygo, O.L. Catalytic performance of structured packages coated with perovskite-based nanocomposite in the methane steam reforming reaction. *Int. J. Hydrogen Energy* **2016**, *41*, 4632–4645. [CrossRef]

85. Shoynkhorova, T.B.; Rogozhnikov, V.N.; Ruban, N.V.; Shilov, V.A.; Potemkin, D.I.; Simonov, P.A.; Belyaev, V.D.; Snytnikov, P.V.; Sobyanin, V.A. Composite Rh/$Zr_{0.25}Ce_{0.75}O_{2-\delta}$-$\gamma$-$Al_2O_3$/Fecralloy wire mesh honeycomb module for natural gas, LPG and diesel catalytic conversion to syngas. *Int. J. Hydrogen Energy* **2019**, *44*, 9941–9948. [CrossRef]

86. Smorygo, O.L.; Sadykov, V.A.; Bobrova, L.N. *Open Cell Foams as Substrates for Design of Structured Catalysts, Solid Oxide Fuel Cells and Supported Asymmetric Membrane*; Nova Science Publishers: Hauppauge, NY, USA, 2016; p. 207.

87. Sadykov, V.A. (Ed.) *Advanced Nanomaterials for Catalysis and Energy. Synthesis, Characterization and Applications*, 1st ed.; Elsevier: Amsterdam, The Netherlands, 2019; p. 567.

88. Pechini, M.P. Method of Preparing Lead and Alkaline Earth Titanates and Niobates and Coating Method Using the Same to Form a Capacitor. US Patent No. 3330697, 1967. Available online: https://patents.google.com/patent/US3330697A/ (accessed on 6 August 2021).

89. Sadykov, V.A.; Simonov, M.N.; Mezentseva, N.V.; Pavlova, S.N.; Fedorova, Y.E.; Bobin, A.S.; Bespalko, Y.N.; Ishchenko, A.V.; Krieger, T.A.; Glazneva, T.S.; et al. Ni-loaded nanocrystalline ceria-zirconia solid solutions prepared via modified Pechini route as stable to coking catalysts of CH_4 dry reforming. *Open Chem.* **2016**, *14*, 363–376. [CrossRef]

90. Sadykov, V.; Pavlova, S.; Smal, E.; Arapova, M.; Simonov, M.; Mezentseva, N.; Rogov, V.; Glazneva, T.; Lukashevich, A.; Roger, A.-C.; et al. Structured catalysts for biofuels transformation into syngas with active components based on perovskite and spinel oxides supported on Mg-doped alumina. *Catal. Today* **2017**, *293–294*, 176–185. [CrossRef]

91. Sadykov, V.; Mezentseva, N.; Fedorova, Y.; Lukashevich, A.; Pelipenko, V.; Kuzmin, V.; Simonov, M.; Ishchenko, A.; Vostrikov, Z.; Bobrova, L.; et al. Structured catalysts for steam/autothermal reforming of biofuels on heat-conducting substrates: Design and performance. *Catal. Today* **2015**, *251*, 19–27. [CrossRef]

92. Shmakov, A.N.; Cherepanova, S.V.; Zyuzin, D.A.; Fedorova, Y.E.; Bobrikov, I.A.; Roger, A.-C.; Adamski, A.; Sadykov, V.A. The crystal structure of compositionally homogeneous mixed ceria-zirconia oxides by high resolution X-ray and neutron diffraction methods. *Open Chem.* **2017**, *15*, 438–445. [CrossRef]

93. Kol'ko, V.P.; Zyuzin, D.A.; Sadykov, V.A.; Kriventsov, V.V.; Moroz, E.M. Structure of the mixed oxides $Me_x(Ce_{0.5}Zr_{0.5})_{1-x}O_y$ (Me = Gd, Pr). *Glass Phys. Chem.* **2007**, *33*, 335–339. [CrossRef]

94. Sadykov, V.A.; Kriventsov, V.V.; Moroz, E.M.; Borchert, Y.V.; Zyuzin, D.A.; Kol'ko, V.P.; Kuznetsova, T.G.; Ivanov, V.P.; Boronin, A.I.; Mezentseva, N.V.; et al. Ceria-zirconia nanoparticles doped with La or Gd: Effect of the doping cation on the real structure. *Solid State Phenom.* **2007**, *128*, 81–88. [CrossRef]

95. Sadykov, V.A.; Mezentseva, N.V.; Alikina, G.M.; Lukashevich, A.I.; Borchert, Y.V.; Kuznetsova, T.G.; Ivanov, V.P.; Trukhan, S.N.; Paukshtis, E.A.; Muzykantov, V.S.; et al. Pt-supported nanocrystalline ceria-zirconia doped with La, Pr or Gd: Factors controlling syngas generation in partial oxidation/autothermal reforming of methane or oxygenates. *Solid State Phenom.* **2007**, *128*, 239–248. [CrossRef]

96. Sadykov, V.; Mezentseva, N.; Alikina, G.; Lukashevich, A.; Muzykantov, V.; Bunina, R.; Boronin, A.; Pazhetnov, E.; Paukshtis, E.; Kriventsov, V.; et al. Doped nanocrystalline Pt-promoted ceria-zirconia as anode catalysts for IT-SOFC: Synthesis and properties. *Mater. Res. Soc. Symp. Proc.* **2007**, *1023*, 26–31. [CrossRef]

97. Kuznetsova, T.G.; Sadykov, V.A. Specific features of the defect structure of metastable nanodisperse ceria, zirconia, and related materials. *Kinet. Catal.* **2008**, *49*, 840–858. [CrossRef]

98. Cortés Corberán, V.; Rives, V.; Mezentseva, N.V.; Sadykov, V.A.; Martínez-Tamayo, E. Nanostructured metal oxide catalyst. In *Nanotechnology for Sustainable Manufacturing*; Rickerby, D., Ed.; CRC Press: Boca Raton, FL, USA, 2014; pp. 153–198.

99. Bulgakov, N.N.; Sadykov, V.A.; Lunin, V.V.; Kemnitz, E. Lattice defects and oxygen absorption/migration in ceria/ceria-zirconia solid solutions: Analysis by semiempirical interacting bonds method. *React. Kinet. Catal. Lett.* **2002**, *76*, 103–110. [CrossRef]

100. Bulgakov, N.N.; Sadykov, V.A.; Lunin, V.V.; Kemnitz, E. Surface energies and heats of oxygen adsorption in ceria/ceria-zirconia solid solutions: Analysis by semiempirical interacting bonds method. *React. Kinet. Catal. Lett.* **2002**, *76*, 111–116. [CrossRef]

101. Sadykov, V.; Rogov, V.; Ermakova, E.; Arendarsky, D.; Mezentseva, N.; Alikina, G.; Sazonova, N.; Bobin, A.; Pavlova, S.; Schuurman, Y.; et al. Mechanism of CH_4 dry reforming by pulse microcalorimetry: Metal nanoparticles on perovskite/fluorite supports with high oxygen mobility. *Thermochim. Acta* **2013**, *567*, 27–34. [CrossRef]

102. Simonov, M.N.; Rogov, V.A.; Smirnova, M.Y.; Sadykov, V.A. Pulse microcalorimetry study of methane dry reforming reaction on Ni/ceria-zirconia catalyst. *Catalysts* **2017**, *7*, 268. [CrossRef]

103. Simonov, M.N.; Sadykov, V.A.; Rogov, V.A.; Bobin, A.S.; Sadovskaya, E.M.; Mezentseva, N.V.; Ishchenko, A.V.; Krieger, T.A.; Roger, A.-C.; van Veen, A.C. Ethanol selective oxidation into syngas over Pt-promoted fluorite-like oxide: SSITKA and pulse microcalorimetry study. *Catal. Today* **2016**, *277*, 157–163. [CrossRef]

104. Sadykov, V.A.; Eremeev, N.F.; Sadovskaya, E.M.; Chesalov, Y.A.; Pavlova, S.N.; Rogov, V.A.; Simonov, M.N.; Bobin, A.S.; Glazneva, T.S.; Smal, E.A.; et al. Detailed mechanism of ethanol transformation into syngas on catalysts based on mesoporous $MgAl_2O_4$ support loaded with Ru+Ni/(PrCeZrO or $MnCr_2O_4$) active components. *Top. Catal.* **2020**, *63*, 166–177. [CrossRef]

105. Sadykov, V.; Sadovskaya, E.; Bobin, A.; Kharlamova, T.; Uvarov, N.; Ulikhin, A.; Argirusis, C.; Sourkouni, G.; Stathopoulos, V. Temperature-programmed $C^{18}O_2$ SSITKA for powders of fast oxide-ion conductors: Estimation of oxygen self-diffusion coefficients. *Solid State Ionics* **2015**, *271*, 69–72. [CrossRef]

106. Sadykov, V.; Eremeev, N.; Sadovskaya, E.; Bobin, A.; Ishchenko, A.; Pelipenko, V.; Muzykantov, V.; Krieger, T.; Amanbaeva, D. Oxygen mobility and surface reactivity of $PrNi_{1-x}Co_xO_{3-\delta}$ perovskites and their nanocomposites with $Ce_{0.9}Y_{0.1}O_{2-\delta}$ by temperature-programmed isotope exchange experiments. *Solid State Ionics* **2015**, *273*, 35–40. [CrossRef]

107. Sadovskaya, E.M.; Ivanova, Y.A.; Pinaeva, L.G.; Grasso, G.; Kuznetsova, T.G.; van Veen, A.; Sadykov, V.A.; Mirodatos, C. Kinetics of oxygen exchange over CeO_2-ZrO_2 fluorite-based catalysts. *J. Phys. Chem. A* **2007**, *111*, 4498–4505. [CrossRef]

108. Pinaeva, L.G.; Sadovskaya, E.M.; Ivanova, Y.A.; Kuznetsova, T.G.; Prosvirin, I.P.; Sadykov, V.A.; Schuurman, Y.; van Veen, A.C.; Mirodatos, C. Water gas shift and partial oxidation of CH_4 over CeO_2–ZrO_2(–La_2O_3) and Pt/CeO_2–ZrO_2(–La_2O_3): Performance under transient conditions. *Chem. Eng. J.* **2014**, *257*, 281–291. [CrossRef]

109. Sadykov, V.A.; Sazonova, N.N.; Bobin, A.S.; Muzykantov, V.S.; Gubanova, E.L.; Alikina, G.M.; Lukashevich, A.I.; Rogov, V.A.; Ermakova, E.N.; Sadovskaya, E.M.; et al. Partial oxidation of methane on Pt-supported lanthanide doped ceria-zirconia oxides: Effect of the surface/lattice oxygen mobility on catalytic performance. *Catal. Today* **2011**, *169*, 125–137. [CrossRef]

110. Reshetnikov, S.I.; Lukashevich, A.I.; Alikina, G.M.; Sadykov, V.A. Effect of oxygen mobility in solid catalyst on transient regimes of catalytic reaction of methane partial oxidation at short contact times. *Catal. Lett.* **2006**, *110*, 235–242. [CrossRef]

111. Pavlova, S.N.; Sazonova, N.N.; Sadykov, V.A.; Alikina, G.M.; Lukashevich, A.I.; Gubanova, E.L.; Bunina, R.V. Study of synthesis gas production over structured catalysts based on LaNi(Pt)O$_x$- and Pt(LaPt)- CeO_2-ZrO_2 supported on corundum. *Stud. Surf. Sci. Catal.* **2007**, *167*, 343–348.

112. Sazonova, N.N.; Sadykov, V.A.; Bobin, A.S.; Pokrovskaya, S.A.; Gubanova, E.L.; Mirodatos, C. Dry reforming of methane over fluorite-like mixed oxides promoted by Pt. *React. Kinet. Catal. Lett.* **2009**, *98*, 35–41. [CrossRef]

113. Yaseneva, P.; Pavlova, S.; Sadykov, V.; Alikina, G.; Lukashevich, A.; Rogov, V.; Belochapkine, S.; Ross, J. Combinatorial approach to the preparation and characterization of catalysts for biomass steam reforming into syngas. *Catal. Today* **2008**, *137*, 23–28. [CrossRef]

114. Wei, T.; Jia, L.; Zheng, H.; Chi, B.; Pu, J.; Li, J. $LaMnO_3$-based perovskite with *in-situ* exsolved Ni nanoparticles: A highly active, performance stable and coking resistant catalyst for CO_2 dry reforming of CH_4. *Appl. Catal. A.* **2018**, *564*, 199–207. [CrossRef]

115. Arapova, M.V.; Pavlova, S.N.; Rogov, V.A.; Krieger, T.A.; Ishchenko, A.V.; Roger, A.-C. Ni(Co)-containing catalysts based on perovskite-like ferrites for steam reforming of ethanol. *Catal. Sustain. Energy* **2014**, *1*, 10–20. [CrossRef]

116. Marinho, A.L.A.; Rabelo-Neto, R.C.; Noronha, F.B.; Mattos, L.V. Steam reforming of ethanol over Ni-based catalysts obtained from $LaNiO_3$ and $LaNiO_3$/$CeSiO_2$ perovskite-type oxides for the production of hydrogen. *Appl. Catal. A Gen.* **2016**, *520*, 53–64. [CrossRef]

117. Sadykov, V.; Sobyanin, V.; Mezentseva, N.; Alikina, G.; Vostrikov, Z.; Fedorova, Y.; Pelipenko, V.; Usoltsev, V.; Tikhov, S.; Salanov, A.; et al. Transformation of CH_4 and liquid fuels into syngas on monolithic catalysts. *Fuel* **2010**, *89*, 1230–1240. [CrossRef]

118. Frolova-Borchert, Y.V.; Sadykov, V.A.; Alikina, G.M.; Lukashevich, A.I.; Moroz, E.M.; Kochubey, D.I.; Kriventsov, V.V.; Zaikovskii, V.I.; Zyryanov, V.V.; Uvarov, N.F. Nanocomposites comprised of doped cerium dioxide and lanthanum manganite for syngas production. *Solid State Ionics* **2006**, *177*, 2533–2538. [CrossRef]

119. Sadykov, V.; Mezentseva, N.; Alikina, G.; Bunina, R.; Rogov, V.; Krieger, T.; Belochapkine, S.; Ross, J. Composite catalytic materials for steam reforming of methane and oxygenates: Combinatorial synthesis, characterization and performance. *Catal. Today* **2009**, *145*, 127–137. [CrossRef]

120. Sadykov, V.; Mezentseva, N.; Alikina, G.; Bunina, R.; Pelipenko, V.; Lukashevich, A.; Tikhov, S.; Usoltsev, V.; Vostrikov, Z.; Bobrenok, O.; et al. Nanocomposite catalysts for internal steam reforming of methane and biofuels in solid oxide fuel cells: Design and performance. *Catal Today.* **2009**, *146*, 132–140. [CrossRef]

121. Sadykov, V.A.; Chub, O.V.; Chesalov, Y.A.; Mezentseva, N.V.; Pavlova, S.N.; Arapova, M.V.; Rogov, V.A.; Simonov, M.N.; Roger, A.-C.; Parkhomenko, K.V.; et al. Mechanism of ethanol steam reforming over Pt/(Ni+Ru)-promoted oxides by FTIRS in situ. *Top. Catal.* **2016**, *59*, 1332–1342. [CrossRef]

122. Marinho, A.L.A.; Toniolo, F.S.; Noronha, F.B.; Epron, F.; Duprez, D.; Bion, N. Highly active and stable Ni dispersed on mesoporous CeO_2-Al_2O_3 catalysts for production of syngas by dry reforming of methane. *Appl. Catal. B Environ.* **2021**, *281*, 119459. [CrossRef]

123. Guilhaume, N.; Bianchi, D.; Wandawa, R.A.; Yin, W.; Yves Schuurman, Y. Study of CO_2 and H_2O adsorption competition in the combined dry/steam reforming of biogas. *Catalysis Today* **2021**, *375*, 282–289. [CrossRef]

124. Di Michele, A.; Dell'Angelo, A.; Tripodi, A.; Bahadori, E.; Sanchez, F.; Motta, D.; Dimitratos, N.; Rossetti, I.; Ramis, G. Steam reforming of ethanol over $Ni/MgAl_2O_4$ catalysts. *Int. J. Hydrogen Energy* **2019**, *44*, 952–964. [CrossRef]

125. Zhang, S.; Ying, M.; Yu, J.; Zhan, W.; Wang, L.; Guo, Y.; Guo, Y. $Ni_xAl_1O_{2-\delta}$ mesoporous catalysts for dry reforming of methane: The special role of $NiAl_2O_4$ spinel phase and its reaction mechanism. *Appl. Catal. B Environ.* **2021**, *291*, 120074. [CrossRef]

126. Lino, A.V.P.; Assaf, E.M.; Assaf, J.M. X-ZrO_2 addition (X= Ce, La, Y and Sm) on $Ni/MgAl_2O_4$ applied to methane tri-reforming for syngas production. *J. CO_2 Util.* **2019**, *33*, 273–283. [CrossRef]

127. Mao, X.; Foucher, A.C.; Stach, E.A.; Gorte, R.J. Changes in Ni-NiO equilibrium due to $LaFeO_3$ and the effect on dry reforming of CH_4. *J. Catal.* **2020**, *381*, 561–569. [CrossRef]

128. Messaoudia, H.; Thomas, S.; Djaidja, A.; Slyemia, S.; Barama, A. Study of La_xNiO_y and $La_xNiO_y/MgAl_2O_4$ catalysts in dry reforming of methane. *J. CO_2 Util.* **2018**, *24*, 40–49. [CrossRef]

129. Pavlova, S.; Fedorova, Y.; Ishchenko, A.; Melgunov, M.; Melgunova, E.; Simonov, M.; Rogov, V.; Krieger, T.; Sadykov, V.; Roger, A.-C. Ni-containing catalysts based on ordered mesoporous MgO–Al_2O_3 for methane dry reforming. *Catal. Sustain. Energy* **2018**, *5*, 59–66. [CrossRef]

130. Jabbour, K.; El Hassan, N.; Davidson, A.; Casaleb, S.; Massiani, P. Factors affecting the long-term stability of mesoporous nickel-based catalysts in combined steam and dry reforming of methane. *Catal. Sci. Technol.* **2016**, *6*, 4616–4631. [CrossRef]

131. Xu, L.; Song, H.; Chou, L. Carbon dioxide reforming of methane over ordered mesoporous NiO–MgO–Al_2O_3 composite oxides. *Appl. Catal. B Environ.* **2011**, *108–109*, 177–190. [CrossRef]

132. Xu, L.; Song, H.; Chou, L. Ordered mesoporous MgO-Al_2O_3 composite oxides supported Ni based catalysts for CO_2 reforming of CH_4: Effects of basic modifier and mesopore structure. *Int. J. Hydrogen Energy* **2013**, *38*, 7307–7325. [CrossRef]

133. Jabbour, K.; Massiani, P.; Davidson, A.; Casale, S.; El Hassan, N. Ordered mesoporous "one-pot" synthesized Ni-Mg(Ca)-Al_2O_3 as effective and remarkably stable catalysts for combined steam and dry reforming of methane (CSDRM). *Appl. Catal. B Environ.* **2017**, *201*, 527–554. [CrossRef]

134. Bobin, A.S.; Sadykov, V.A.; Rogov, V.A.; Mezentseva, N.V.; Alikina, G.M.; Sadovskaya, E.M.; Glazneva, T.S.; Sazonova, N.N.; Smirnova, M.Y.; Veniaminov, S.A.; et al. Mechanism of CH_4 dry reforming on nanocrystalline doped ceria–zirconia with supported Pt, Ru, Ni, and Ni–Ru. *Top. Catal.* **2013**, *56*, 958–968. [CrossRef]

135. Sadykov, V.A.; Tikhov, S.F.; Isupova, L.A. *Heterogeneous Catalytic Redox Reactions*; De Gruyter: Berlin, Germany; Boston, MA, USA, 2020.

136. Sadykov, V.A.; Gubanova, E.L.; Sazonova, N.N.; Pokrovskaya, S.A.; Chumakova, N.A.; Mezentseva, N.V.; Bobin, A.S.; Gulyaev, R.V.; Ishchenko, A.V.; Krieger, T.A.; et al. Dry reforming of methane over Pt/PrCeZrO catalyst: Kinetic and mechanistic features by transient studies and their modeling. *Catal. Today* **2011**, *171*, 140–149. [CrossRef]

137. Sadykov, V.; Mezentseva, N.; Muzykantov, V.; Efremov, D.; Gubanova, E.; Sazonova, N.; Bobin, A.; Paukshtis, E.; Ishchenko, A.; Voronin, V.; et al. Real structure-oxygen mobility relationship in nanocrystalline doped ceria-zirconia fluorite-like solid solutions promoted by Pt. *MRS Online Proc. Libr.* **2008**, *1122*, 1122-O05-03. [CrossRef]

138. Ulianitsky, V.; Shtertser, A.; Sadykov, V.; Smurov, I. Development of catalytic converters using detonation spraying. *Mater. Manuf. Process.* **2016**, *31*, 1433–1438. [CrossRef]

139. Rogozhnikov, V.N.; Kuzin, N.A.; Snytnikov, P.V.; Potemkin, D.I.; Shoynkhorova, T.B.; Simonov, P.A.; Shilov, V.A.; Ruban, N.V.; Kulikov, A.V.; Sobyanin, V.A. Design, scale-up, and operation of a $Rh/Ce_{0.75}Zr_{0.25}O_{2-\delta}$-η-$Al_2O_3$/FeCrAl alloy wire mesh honeycomb catalytic module in diesel autothermal reforming. *Chem. Eng. J.* **2019**, *374*, 511–519. [CrossRef]

140. Zazhigalov, S.V.; Rogozhnikov, V.N.; Snytnikov, P.V.; Potemkin, D.I.; Simonov, P.A.; Shilov, V.A.; Ruban, N.V.; Kulikov, A.V.; Zagoruiko, A.N.; Sobyanin, V.A. Simulation of diesel autothermal reforming over $Rh/Ce_{0.75}Zr_{0.25}O_{2-\delta}$-η-$Al_2O_3$/FeCrAl wire mesh honeycomb catalytic module. *Chem. Eng. Process.* **2020**, *150*, 107876. [CrossRef]

141. Potemkin, D.I.; Rogozhnikov, V.N.; Ruban, N.V.; Shilov, V.A.; Simonov, P.A.; Shashkov, M.V.; Sobyanin, V.A.; Snytnikov, P.V. Comparative study of gasoline, diesel and biodiesel autothermal reforming over Rh-based FeCrAl-supported composite catalyst. *Int. J. Hydrogen Energy* **2020**, *45*, 26197–26205. [CrossRef]
142. Shilov, V.A.; Rogozhnikov, V.N.; Zazhigalov, S.V.; Potemkin, D.I.; Belyaev, V.D.; Shashkov, M.V.; Zagoruiko, A.N.; Sobyanin, V.A.; Snytnikov, P.V. Operation of $Rh/Ce_{0.75}Zr_{0.25}O_{2-\delta}$-η-$Al_2O_3$/FeCrAl wire mesh honeycomb catalytic modules in diesel steam and autothermal reforming. *Int. J. Hydrogen Energy* **2021**, in press. [CrossRef]